

## Application of the small-tip-angle approximation in the toggling frame for the design of analytic robust pulses in quantum control

L. Van Damme <sup>1,\*</sup>, D. Sugny <sup>2,†</sup> and S. J. Glaser <sup>1,3,‡</sup>

<sup>1</sup>*Department of Chemistry, Technical University of Munich, Lichtenbergstrasse 4, D-85747 Garching, Germany*

<sup>2</sup>*Laboratoire Interdisciplinaire Carnot de Bourgogne (ICB), UMR 6303 CNRS-Université de Bourgogne-Franche Comté, 9 Avenue A. Savary, B.P. 47 870, F-21078 Dijon Cedex, France*

<sup>3</sup>*Munich Center for Quantum Science and Technology (MCQST), Schellingstrasse 4, 80799 München, Germany*



(Received 12 August 2021; accepted 14 October 2021; published 28 October 2021)

We apply the small-tip-angle approximation in the toggling frame in order to analytically design robust pulses against resonance offsets for state to state transfer in two-level quantum systems. We show that a broadband or a local robustness up to an arbitrary order can be achieved. We provide different control parametrizations to satisfy experimental constraints and limitations on the amplitude or energy of the pulse. A comparison with numerical optimal solutions is made.

DOI: [10.1103/PhysRevA.104.042226](https://doi.org/10.1103/PhysRevA.104.042226)

### I. INTRODUCTION

Manipulating quantum systems by means of time-dependent external controls has been a topic of increasing interest in the past decades. It has become a well-recognized field of research with applications ranging from molecular physics [1–3] to nuclear magnetic resonance (NMR) [4–9] and nowadays quantum technologies [4,10,11]. In this context, progress has been made for the design of efficient pulses able to realize specific tasks. On the theoretical side, such advances extend from the discovery of elementary basic mechanisms of field-induced dynamics such as adiabatic protocols [12], to shortcut to adiabaticity [13–16] and optimal control procedures [17–24], which have made possible the control of systems of growing complexity. However, in order to be effective for experimental applications, such open-loop control methods require the accurate knowledge of system dynamics. This problem can be solved by considering pulses robust against variations of specific parameters of the system [25]. The basic idea is generally to consider the simultaneous control of an ensemble of quantum systems which differ by the value of one or several parameters. A large amount of solutions have been proposed in the literature to date, with their own advantages and limitations [26] in terms of pulse duration and energy or efficiency of the control protocol. Among recent propositions for two-level quantum systems, we mention composite pulses [27–31], procedures based on shortcut controls [32–34], learning control [35,36], and optimal control methods [4,37–44]. As an illustrative example of this control issue, we consider in this study the control of two-level quantum systems with different resonance

offsets, which can be viewed as a reference problem for robust protocols in quantum control.

In this context, the design of robust pulses is a nontrivial task due to the bilinearity of the controlled Schrödinger (or Bloch) equation. Ideally, the system dynamics and the corresponding control should be expressed in terms of simple functions with a minimum number of free parameters. This aspect is important to reveal the control mechanism or to apply quickly and efficiently the control protocols in a given experimental setup. However, the time evolution of the Schrödinger equation for two-level quantum systems can be analytically computed only for some simple controls, such as constant pulses with a constant phase. Most of the robust pulses have therefore been built on the basis of numerical optimizations of a large number of parameters, for which the integration of the dynamics is made by a numerical propagation. Analytical studies of the control of an ensemble of two-level quantum systems is much more difficult and requires in general some approximations to simplify the dynamics. For this purpose, average Hamiltonian theory (AHT) [45,46] uses a Magnus expansion to express the propagator. This expansion becomes extremely complicated above the second order, which limits the efficiency of this approach. The small-tip-angle approximation (STA) [5,47] is another way to deal with the control problem and gives interesting results for state to state transfers. STA linearizes the Bloch equation which allows one to compute explicitly its solutions. However, this method only works for transfers involving relatively small flip angles on the Bloch sphere and not, e.g., for an inversion process. The combination of STA and optimal control has been recently investigated in detail [16,48]. These two methods are much more efficient in the so-called *toggling frame* (or interaction frame) [45,46], hereafter denoted TF. The latter is a time-dependent frame which follows the state of a resonant spin. Recently, Zeng *et al.* published a series of papers about the application of AHT in TF [49–51]. They found a way to improve the pulse robustness by making use of three-dimensional

\*leo.vandamme@gmx.fr

†dominique.sugny@u-bourgogne.fr

‡glaser@tum.de

curves derived from the first-order Magnus expansion. Their procedure allows one to control the robustness of unitary gates by canceling the effect of offset inhomogeneities in higher and higher orders of the Magnus expansion. Due to its complexity, the computation of high orders requires numerical techniques. Moreover, this method improves *locally* the robustness (i.e., for small resonance offsets), but, as far as we know, broadband robust pulses for a large range of frequencies cannot be derived.

In this paper, we propose to revisit this approach by applying STA in TF. Many original results can be found for state to state transfers. This method has the decisive advantage of being simpler and more efficient than AHT, even if its generalization to unitary transformations seems more difficult. This paper focuses mainly on robust inversion pulses against offset inhomogeneities (or  $B_0$  inhomogeneities), but we show that our approach can be generalized to any state to state transfer. The evaluation of the robustness is made through the distance of the final state to the target one as a function of the offset parameter relative to the resonance frequency. This description corresponds to the current experimental uncertainties that can be encountered in molecular physics, NMR, or quantum technologies. We consider two different definitions of robustness, either global or local. In the first case, the problem is to control an inhomogeneous ensemble of spins of different offsets, while in the second framework the system is expanded order by order with respect to the offset parameter.

The paper is organized as follows. In Sec. II, we introduce the model system and we express its dynamics in TF by using STA. We also describe the general methodology used to design robust control pulses. Section III is mainly dedicated to the inversion process. We derive a series of analytical solutions both with broadband or local robustness properties. A generalization to any state to state transfer is presented in Sec. III C. A comparison with numerical optimal control protocols is presented in Sec. IV. Conclusion and prospective views are given in Sec. V. Technical details are reported in Appendixes A, B, and C.

## II. METHODOLOGY

### A. Model system

We consider an inhomogeneous ensemble of uncoupled two-level quantum systems with different resonance offsets neglecting relaxation. In a given rotating frame, the dynamics of the Bloch vector describing the state of a system are given by

$$\dot{\vec{M}}(\delta, t) = [H_0(t) + \delta H_1] \vec{M}(\delta, t), \quad (1)$$

with

$$H_0(t) = \begin{pmatrix} 0 & 0 & -u_y(t) \\ 0 & 0 & u_x(t) \\ u_y(t) & -u_x(t) & 0 \end{pmatrix}, \quad (2)$$

$$H_1 = \begin{pmatrix} 0 & 1 & 0 \\ -1 & 0 & 0 \\ 0 & 0 & 0 \end{pmatrix},$$

where  $\delta$  is the resonance offset and  $u_x(t)$  and  $u_y(t)$  are the components of the control pulse. The control would be in-

finately robust if  $\vec{M}(\delta, T)$  reaches a given target state for all  $\delta$ . For an inversion pulse, the cost profile (i.e., the error of the transfer as a function of  $\delta$ ) is measured by

$$J_{\text{BLOCH}}(\delta) = 1 + M_z(\delta, T), \quad (3)$$

which is zero if the inversion is perfectly realized for an offset  $\delta$  [we have in this case  $M_z(\delta, T) = -1$ ] and 2 if the spin is not excited at all. TF (or interaction frame) [46,52,53] is defined by a propagator whose dynamics are governed by  $H_0$  only. In other words, it corresponds to a rotation matrix  $R_0 \in \text{SO}(3)$  which fulfills  $\dot{R}_0 = H_0 R_0$ .  $R_0$  is an orthogonal  $3 \times 3$  matrix that can be expressed as

$$R_0(t) = \begin{pmatrix} q_x(t) & q_y(t) & q_z(t) \\ p_x(t) & p_y(t) & p_z(t) \\ v_x(t) & v_y(t) & v_z(t) \end{pmatrix}, \quad (4)$$

where we have introduced the vectors  $\vec{q} = (q_x, q_y, q_z)^\top$ ,  $\vec{p} = (p_x, p_y, p_z)^\top$ , and  $\vec{v} = (v_x, v_y, v_z)^\top$ . These vectors correspond to the three axes of the original frame expressed in the toggling frame. The vector  $\vec{q}$  is the  $x$  axis of the original frame expressed in TF,  $\vec{p}$  is the  $y$  axis, and  $\vec{v}$  is the  $z$  axis. Since initially we have  $R_0(0) = \mathbb{I}$  (the two frames are equal at the beginning of the process), we obtain  $\vec{q}(0) = (1, 0, 0)^\top$ ,  $\vec{p}(0) = (0, 1, 0)^\top$ , and  $\vec{v}(0) = (0, 0, 1)^\top$ . We denote as  $\vec{L}$  the Bloch vector described in TF, i.e., such that its components  $L_x$ ,  $L_y$ , and  $L_z$  correspond to the projection of  $\vec{M}$  onto the three axes of TF. The dynamics of  $\vec{L}$  can be derived by applying the transformation  $\vec{L} = R_0^\top \vec{M}$ . Using Eq. (1), we obtain

$$\dot{\vec{L}}(\delta, t) = \delta \tilde{H}_1(t) \vec{L}(\delta, t), \quad (5)$$

where  $\tilde{H}_1 = R_0^\top H_1 R_0$  is the so-called interaction Hamiltonian. Since  $R_0$  is an orthogonal matrix, we deduce that  $\vec{q} \times \vec{p} = \vec{v}$ , which allows one to explicitly write  $\tilde{H}_1$  as

$$\tilde{H}_1(t) = \begin{pmatrix} 0 & v_z(t) & -v_y(t) \\ -v_z(t) & 0 & v_x(t) \\ v_y(t) & -v_x(t) & 0 \end{pmatrix}. \quad (6)$$

Note that, at the resonance, we have  $\dot{\vec{L}}(\delta = 0, t) = 0$ , i.e., the Bloch vector is a constant of the motion. This vector stays along the  $z$  axis of TF during the dynamics. Since the dynamics of  $R_0$  are controllable, the functions  $v_x$ ,  $v_y$ , and  $v_z$  can be chosen arbitrarily and Eq. (5) can be viewed as a new control problem, where  $v_x$ ,  $v_y$ , and  $v_z$  are the new control variables. Note that, in the system (5), the interaction Hamiltonian generates rotations about  $\vec{v}$ ; hence  $\vec{v}$  can be seen as a control pulse by analogy with the transverse control field in the original Bloch equation. The fact that  $R_0$  is orthogonal leads to the constraint

$$v_x^2(t) + v_y^2(t) + v_z^2(t) = 1. \quad (7)$$

As we explained above, the vector  $\vec{v}$  is also equal to the unit vector along the  $z$  axis of the laboratory frame (see Fig. 1). It can be shown that the original pulse can be computed from  $\vec{v}$  as [51]

$$\Omega(t) = \|\dot{\vec{v}}(t)\|, \quad \phi(t) = \int_0^t \frac{[\vec{v}(t') \times \dot{\vec{v}}(t')] \cdot \ddot{\vec{v}}(t')}{\Omega^2(t')} dt', \quad (8)$$

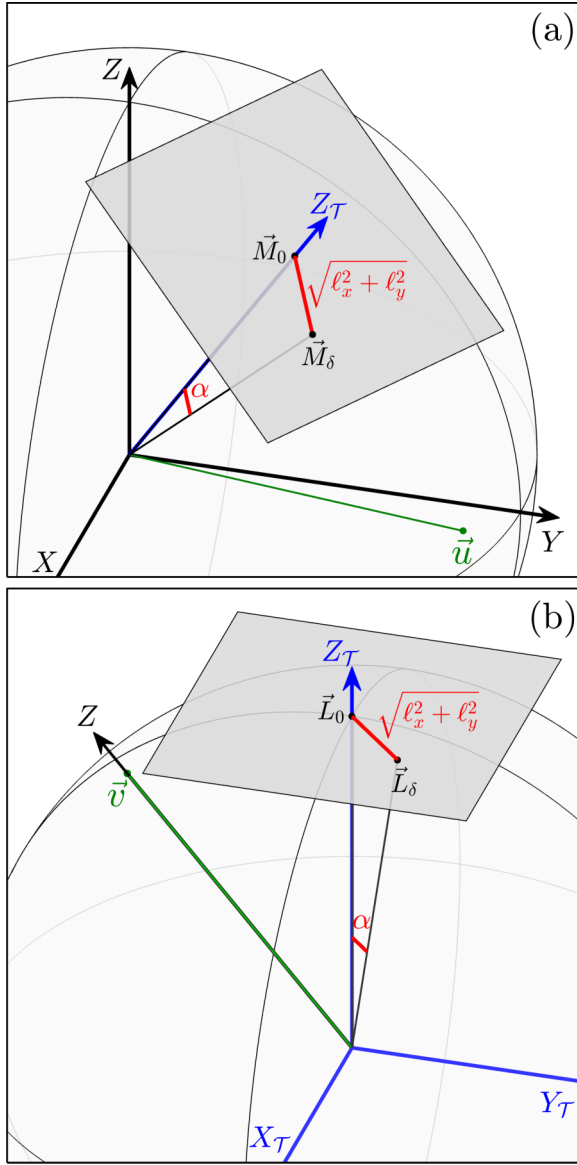


FIG. 1. Panel (a): representation of the  $z$  axis of TF ( $Z_T$  in blue or dark gray) moving on the Bloch sphere together with a resonant Bloch vector  $\vec{M}_0 \equiv \vec{M}(0, t)$  and a nonresonant one  $\vec{M}_\delta \equiv \vec{M}(\delta, t)$ . The vector  $\vec{u}(t)$  is the transverse control  $\vec{u} = (\Omega \cos \phi, \Omega \sin \phi, 0)^T$ . The resonant Bloch vector remains along  $Z_T$  during the whole process. The angle between  $Z_T$  and  $\vec{M}(\delta, t)$  is denoted as  $\alpha(t)$ . If  $\alpha$  is small enough during the dynamics,  $\vec{M}(\delta, t)$  moves approximately in the gray plane and STA holds in TF. The angle  $\alpha(t)$  is measured by  $\sqrt{\ell_x^2(\delta, t) + \ell_y^2(\delta, t)}$ , which is also the distance between  $Z_T$  and  $\vec{M}(\delta, t)$  (red or gray line). Panel (b): representation of the  $z$ -axis of the laboratory frame ( $Z$  in black) moving in TF. In this framework, the vector  $\vec{v}(t)$  plays the role of a pulse (by analogy with  $\vec{u}$  in the original frame) with a norm  $\|\vec{v}\| = 1$ , and remains along  $Z$  during the whole process. Here  $\alpha(t)$  is the polar angle describing the dynamics of  $\vec{L}(\delta, t)$ . The vectors  $\vec{M}$  of panel (a) and  $\vec{L}$  of panel (b) are the same but expressed in different frames. Quantities plotted are dimensionless.

where  $\Omega = \sqrt{u_x^2 + u_y^2}$  and  $\phi = \arctan(u_y/u_x)$  are respectively the amplitude and the phase of the pulse. We stress that  $\Omega$  is the norm of the derivative of  $\vec{v}$  and not the derivative of the norm. Instead of optimizing directly  $u_x(t)$  and  $u_y(t)$ , we can

optimize  $\vec{v}(t)$  in Eqs. (5) and (6) and deduce the pulse through Eq. (8).

### B. Boundary constraints

The main difference between the new dynamical system and the original one is that the vector  $\vec{v}(t)$  must satisfy boundary constraints at  $t = 0$  and  $t = T$ . This point is due to the fact that TF is not a static frame. It has to realize a certain transfer which depends on the target state of the control problem. TF is equal to the original frame at  $t = 0$ , i.e.,  $R_0(0) = \mathbb{I}$ , which, from Eq. (4), leads to

$$\vec{v}(0) = (0, 0, 1)^T, \quad (9)$$

while  $\vec{v}(T)$  depends on the target state. For the design of an inversion pulse, TF has to be flipped, i.e.,  $R_0(T) = \text{diag}(1, -1, -1)$ , leading to

$$\vec{v}(T) = (0, 0, -1)^T. \quad (10)$$

A pulse is said to be robust against offset variations if, for any offset  $\delta$ , the Bloch vector remains in a neighborhood of the  $z$  axis of TF. As explained above, a resonant Bloch vector with  $\delta = 0$  stays exactly along the  $z$  axis of TF during the control process, i.e.,  $\vec{L}(0, t) = (0, 0, 1)^T$ . Ideally, if, at the final time, we have  $\vec{L}(\delta, T) = (0, 0, 1)^T \forall \delta$ , then the associated pulse is infinitely robust. In other words, in TF, a robust control process steers the systems from the  $z$  axis back to the  $z$  axis. The final angle between the Bloch vector and the  $z$  axis of TF is measured by  $\arccos [L_z(\delta, T)]$ . The cost profile can thus be defined as follows:

$$J_{\text{TF}}(\delta) = 1 - L_z(\delta, T), \quad (11)$$

which is zero for a perfect return to the  $z$  axis [ $L_z(\delta, T) = 1$ ]. It is worth noting that the cost does not depend explicitly on the target state, this latter being determined by the final constraint  $\vec{v}(T)$ . For an arbitrary target flip angle  $\theta_T$  on the Bloch sphere, the constraint (10) can be generalized to  $\vec{v}(T) = (\sin[\theta_T], 0, \cos[\theta_T])^T$ , while the cost profile is still given by (11). The azimuthal target angle does not appear in this constraint, but it can be set by adding an appropriate constant to the phase of the pulse.

In general, Eq. (5) is not simpler to solve than the original Bloch equation and does not provide any advantage. However, some approximations can be made such as AHT, which is much more accurate in TF [45,46]. Another solution is to use STA [47], which is particularly efficient for state to state transfers. We show in Sec. II C that it is a very natural approach in this control problem.

### C. Application of the small-tip-angle approximation

A large amount of work has used STA for the design of robust or selective pulses in NMR and magnetic resonance imaging (MRI) due to its very good efficiency in state to state transfers. Among others, we mention the small-tip-angle spokes [54],  $k_T$ -point pulses [55,56], SPINS [57], and fast  $k_z$  pulses [58]. The unit vector  $\vec{L}$  can be represented in polar coordinates as

$$\vec{L} = (\sin \alpha \cos \beta, \sin \alpha \sin \beta, \cos \alpha)^T,$$

with  $\alpha$  being the flip angle and  $\beta$  the azimuthal one. If  $\alpha$  is small enough, we have  $\cos \alpha \simeq 1$  and the vector  $\vec{L}$  moves in a plane tangent to the sphere in  $L_z = 1$ . We thus have  $\vec{L} \simeq \vec{\ell} = (\ell_x, \ell_y, 1)^\top$ , which is however not of norm unity. If needed, the mapping between  $\vec{\ell}$  and  $\vec{L}$  is given by  $\alpha = \sqrt{\ell_x^2 + \ell_y^2}$  and  $\beta = \arctan(\frac{\ell_y}{\ell_x})$ .

STA can be applied for flip angles less than  $30^\circ$  [47], but some studies use this approximation up to  $105^\circ$ , which still works surprisingly well [59,60]. It is particularly relevant in TF. Since the resonant Bloch vector is static and stays along the  $z$  axis of TF, we deduce that, if  $\delta$  is small enough, the corresponding vector stays in a neighborhood of the  $z$  axis of TF, which means that the flip angle remains small. Since STA is valid even for relatively large flip angles, we expect that it can be applied over a relatively large range of offsets. Figure 1 depicts the  $z$  axis of TF, the tangent plane where the STA holds, and the flip angle  $\alpha$ .

A decisive advantage of using STA in TF is that the solution of the Bloch equation can be expressed through a simple integral. The  $z$  component of the Bloch vector  $\vec{L}$  being equal to 1, we deduce from Eq. (5) that the dynamics of the  $x$  and  $y$  coordinates are given by

$$\begin{aligned}\dot{\ell}_x(\delta, t) &= \delta[v_z(t)\ell_y(\delta, t) - v_y(t)], \\ \dot{\ell}_y(\delta, t) &= \delta[v_x(t) - v_z(t)\ell_x(\delta, t)].\end{aligned}\quad (12)$$

We consider the complex component  $\ell = \ell_x + i\ell_y$ . We have

$$\dot{\ell}(\delta, t) = -i\delta v_z(t)\ell(\delta, t) + i\delta[v_x(t) + iv_y(t)].\quad (13)$$

Introducing the functions

$$\begin{aligned}k_x(t) &= \int_0^t v_x(t')dt', \\ k_y(t) &= \int_0^t v_y(t')dt', \\ k_z(t) &= \int_0^t v_z(t')dt',\end{aligned}\quad (14)$$

one can check that the solution of (13) is of the form

$$\ell(\delta, T) = i\delta e^{-i\delta k_z(T)} \int_0^T [\dot{k}_x(t) + i\dot{k}_y(t)]e^{i\delta k_z(t)} dt.\quad (15)$$

All the nonlinear properties of the Bloch equations are now contained in the functions  $k_x$ ,  $k_y$ , and  $k_z$ . In this system, the angle between the Bloch vectors and the  $z$  axis of TF is measured by  $\alpha = |\ell|$  with  $|\ell| = \sqrt{\ell_x^2 + \ell_y^2}$ . In order to be consistent with Eq. (11), we define the cost profile as

$$J_{\text{STA}}(\delta) = 1 - \cos[|\ell(\delta, T)|].\quad (16)$$

This cost is nullified for  $|\ell(\delta, T)| = 0$ . Note that it is also equal to 0 when  $|\ell(\delta, T)|$  is a multiple of  $2\pi$ . However, in this later case, the angle between the Bloch vectors and the  $z$  axis of TF is too large to consider STA as a valid approximation. Equation (15) is very similar to the master equation involved in  $k$ -space analysis in MRI [47]. The function  $k_z$  plays here the role of a one-dimensional  $k$  space and  $\dot{k}_x$  and  $\dot{k}_y$  are analog to a rf pulse. However, while in a standard application of STA,  $k_x(t)$ ,  $k_y(t)$ , and  $k_z(t)$  would be independent, here Eq. (7) involves that their derivatives satisfy  $\dot{k}_x^2 + \dot{k}_y^2 + \dot{k}_z^2 =$

1, which might result in difficulties for solving analytically the integral (15). A technique that allows one to overcome this problem is presented in Sec. II E.

#### D. Local robust control

We also consider the robustness against local variations of the offset [33,41,51,61,62]. In this case, since  $\delta \rightarrow 0$ , the solution of the Bloch equation can be approximated by a Taylor series of the form

$$\vec{L}^{(N)}(\delta, t) = \vec{L}_0(t) + \delta\vec{L}_1(t) + \delta^2\vec{L}_2(t) + \dots + \delta^N\vec{L}_N(t).$$

Instead of minimizing a cost function over a certain range of offsets, all the vectors  $\vec{L}_k$  can be canceled up to the order  $k = N$  at the final time to ensure that the inhomogeneities do not disturb the system up to an error  $\delta^N$ . This results in a very good fidelity in a neighborhood of  $\delta = 0$ , i.e., in a local robustness. The method is relevant for our problem since the precision of STA increases as  $\delta$  becomes smaller. Its application is natural in this framework as it consists in truncating the generating series of the exponential of Eq. (15), i.e.,

$$\begin{aligned}\ell^{(N)}(\delta, T) &= i\delta e^{-i\delta k_z(T)} \int_0^T [\dot{k}_x(t) + i\dot{k}_y(t)] \\ &\quad \times \sum_{k=1}^N \frac{[i\delta k_z(t)]^{k-1}}{(k-1)!} dt.\end{aligned}\quad (17)$$

An  $N$ th order robust process is realized by nullifying both the real and imaginary part of this integral, i.e., by finding functions  $k_x(t)$ ,  $k_y(t)$ , and  $k_z(t)$  such that the  $N$  following integrals cancel:

$$C_k \equiv \int_0^T [\dot{k}_x(t) + i\dot{k}_y(t)]k_z^{k-1}(t)dt = 0, \quad k = \{1, \dots, N\}.\quad (18)$$

For  $N = 0$  we have  $\ell^{(0)}(\delta, T) = 0$ , since the Bloch vector stays along the  $z$  axis of TF at the resonance (the transverse component of the Bloch vector is null in TF). Zeng *et al.* have analyzed the problem of local robustness in a series of papers [49–51] through 3D curves that are in our case  $\Gamma = (k_x, k_y, k_z)$ . However, they focused on the geometric properties of these curves and not on the derivation of explicit analytic pulses. The resulting pulses can be of very high peak amplitude, which may make them unrealistic experimentally. We use here a slightly different approach that allows us to find analytic expressions of the controls that are suitable for practical implementation in the case of the robust inversion problem.

#### E. Analytical pulse design

Whether it is for broadband or local robustness purposes, our study consists in finding appropriate functions  $k_x$ ,  $k_y$ ,  $k_z$  and deducing the pulse. In the broadband case, the functions are chosen to improve the cost profile given by Eq. (16) over a wide range of  $\delta$ , while in the local case, they have to cancel the integrals  $C_k$  in Eq. (18). The choice of these functions must nevertheless be made very carefully. The boundary constraints on  $\vec{v}$  described in Sec. II B, which determine the transfer, imply that the time derivative of the functions  $k_x$ ,  $k_y$ , and  $k_z$  fulfill

$\dot{\vec{k}}(0) = (0, 0, 1)^\top$ , and  $\dot{\vec{k}}(T) = (0, 0, -1)^\top$  for an inversion. An additional constraint discussed in Sec. II C is that  $\|\dot{\vec{k}}\| = 1$ .

This latter restricts dramatically the choice of  $\vec{k}(t)$ . Finding a suitable basis of functions satisfying  $\|\vec{k}\| = 1$  is possible only in some simple cases. This problem has been solved in Refs. [49–51] and we use here the same method. For any function  $s$  increasing monotonously from  $s(0) = s_0$  to  $s(T) = s_T$ , it is straightforward to show that the integral (15) can be rewritten as

$$\ell(\delta, T) = i\delta e^{-i\delta k_z(s_T)} \int_{s_0}^{s_T} \left( \frac{dk_x}{ds} + i \frac{dk_y}{ds} \right) e^{i\delta k_z(s)} ds. \quad (19)$$

Therefore, one can choose some functions  $k_x(s)$ ,  $k_y(s)$ , and  $k_z(s)$  such that  $\|d\vec{k}(s)/ds\| \neq 1$ , while the function  $s(t)$  is deduced from  $\|d\vec{k}(t)/dt\| = 1$ . Indeed, we have

$$\left\| \frac{d\vec{k}}{dt} \right\| = 1 \Rightarrow \left\| \frac{d\vec{k}}{ds} \right\| \frac{ds}{dt} = 1 \Rightarrow \left\| \frac{d\vec{k}}{ds} \right\| ds = dt. \quad (20)$$

Integrating from  $s_0$  to  $s$ , we obtain

$$\int_{s_0}^s \left\| \frac{d\vec{k}(s')}{ds'} \right\| ds' = t, \quad (21)$$

while the duration  $T$  of the pulse is given by integrating until  $s = s_T$ . The function  $s(t)$  is thus obtained by inverting this integral, which can be done numerically if necessary. The boundary constraints are also slightly relaxed. For an inversion, it is now sufficient to select functions such that

$$\begin{aligned} \frac{dk_x}{ds} = 0, \quad \frac{dk_y}{ds} = 0, \quad \frac{dk_z}{ds} > 0 \quad \text{at } s = s_0, \\ \frac{dk_x}{ds} = 0, \quad \frac{dk_y}{ds} = 0, \quad \frac{dk_z}{ds} < 0 \quad \text{at } s = s_T. \end{aligned} \quad (22)$$

Finally, we show in Appendix A that the control pulses given by (8) can be expressed using the formula

$$\begin{aligned} \Omega[s(t)] &= \left\| \frac{d\vec{k}}{ds} \times \frac{d^2\vec{k}}{ds^2} \right\| \left\| \frac{d\vec{k}}{ds} \right\|^{-3}, \\ \phi[s(t)] &= \int_{s_0}^{s(t)} \frac{\left( \frac{d\vec{k}}{ds} \times \frac{d^2\vec{k}}{ds^2} \right) \cdot \frac{d^3\vec{k}}{ds^3}}{\left\| \frac{d\vec{k}}{ds} \times \frac{d^2\vec{k}}{ds^2} \right\|^2} \left\| \frac{d\vec{k}}{ds} \right\| ds. \end{aligned} \quad (23)$$

The advantage of this expression is that it can be derived without knowing explicitly  $s(t)$ . The problem is thus simplified to the search of some functions  $k_x(s)$ ,  $k_y(s)$ , and  $k_z(s)$  under the constraints (22). The derivative  $d\vec{k}/ds$  does not need to belong to  $S^2$ . The pulse is given by (23) and the function  $s(t)$  by (21).

### III. APPLICATION FOR INVERSION PULSES

#### A. Broadband pulses

This section focuses on the broadband case. We propose various parametrizations of  $\vec{k}(s)$  and we derive the pulse according to Eq. (23). The local robust control problem is studied in Secs. III B and III C. Roughly speaking, Eq. (19) suggests that, if  $dk_x/ds$  and  $dk_y/ds$  are two fast oscillating functions, the integral (19) is close to zero as well as the cost profile (16). The main idea of this section is to define a parameter, hereafter referred to as  $\nu$ , which determines the

oscillating frequency of these functions. We expect that the robustness of the pulse increases with  $\nu$ . For each pulse, the robustness is verified using a numerical integration of the original Bloch equation (1) and a computation of the cost profile (3). In all the following results, the bounds of  $s(t)$  are given by

$$s_0 = 0 \longrightarrow s_T = \pi. \quad (24)$$

An infinity of solutions could be derived. Only a few are described in this paper. We stress that the technical computations are not straightforward. The use of a symbolic computation software such as MATHEMATICA [63], XMAXIMA [64], or MAPLE [65] is particularly helpful.

*Anger-Weber solution.* In this paragraph, we present all the steps of the method for the design of a simple analytic inversion pulse. Let us consider some functions  $k_x(s)$ ,  $k_y(s)$ , and  $k_z(s)$  satisfying

$$\begin{aligned} \frac{dk_x}{ds} &= \sin(s) \cos(\nu s), & \frac{dk_y}{ds} &= \sin(s) \sin(\nu s), \\ \frac{dk_z}{ds} &= \cos(s), & k_z(s) &= \sin(s), \end{aligned} \quad (25)$$

where  $\nu$  is an arbitrary parameter introduced above that sets the oscillating frequency of the functions. We can show that the complex transverse component given by Eq. (19) reads

$$\begin{aligned} \ell(\delta, T) &= i\delta \int_0^\pi \sin(s) e^{i\nu s} e^{i\delta \sin(s)} ds \\ &= \frac{\delta}{2} \int_0^\pi \left( e^{i[(\nu+1)s+\delta \sin(s)]} - e^{i[(\nu-1)s+\delta \sin(s)]} \right) ds \\ &= -\frac{\delta\pi e^{i\nu\pi}}{2} [\mathbf{J}_{\nu+1}(\delta) - \mathbf{J}_{\nu-1}(\delta) - i[\mathbf{E}_{\nu+1}(\delta) \\ &\quad - \mathbf{E}_{\nu-1}(\delta)]], \end{aligned} \quad (26)$$

where  $\mathbf{J}$  and  $\mathbf{E}$  are the Anger and Weber functions, respectively [66]. An interesting characteristic of these functions is that, when  $\nu$  increases, both  $\mathbf{E}_\nu(\delta)$  and  $\mathbf{J}_\nu(\delta)$  get closer to zero [and thus  $|\ell(\delta, T)|$  as well] over a wider range of  $\delta$ . Since the cost profile is given by  $1 - \cos[|\ell(\delta, T)|]$  in STA, the parameter  $\nu$  can be used to improve the robustness, as expected (see Fig. 2). To make it more evident, let us consider the case  $\nu \rightarrow \infty$ . We obtain [67]

$$\ell(\delta, T) \underset{\nu \rightarrow \infty}{\simeq} -i\delta \left( \frac{1 + e^{i\nu\pi}}{\nu^2 - 1} - 2\delta \frac{1 - e^{i\nu\pi}}{\nu(\nu^2 - 4)} \right),$$

and we can show that

$$|\ell(\delta, T)| \underset{\nu \rightarrow \infty}{\simeq} 2|\delta| \sqrt{\left[ \frac{\cos\left(\frac{\pi\nu}{2}\right)}{\nu^2 - 1} \right]^2 + \left[ \frac{2\delta \sin\left(\frac{\pi\nu}{2}\right)}{\nu(\nu^2 - 4)} \right]^2}.$$

This latter equation shows that, for a fixed range of  $\delta$ ,  $|\ell(\delta, T)|$  tends to zero as  $\nu$  becomes larger. The cost profile is thus improved. Let us compute the corresponding pulse. The function  $s(t)$  is given by Eq. (21), which leads to

$$s(t) = t, \quad (27)$$

and the total duration is  $T = \pi$ . The amplitude  $\Omega$  and the phase  $\phi$  are derived by using Eq. (23). We used the free

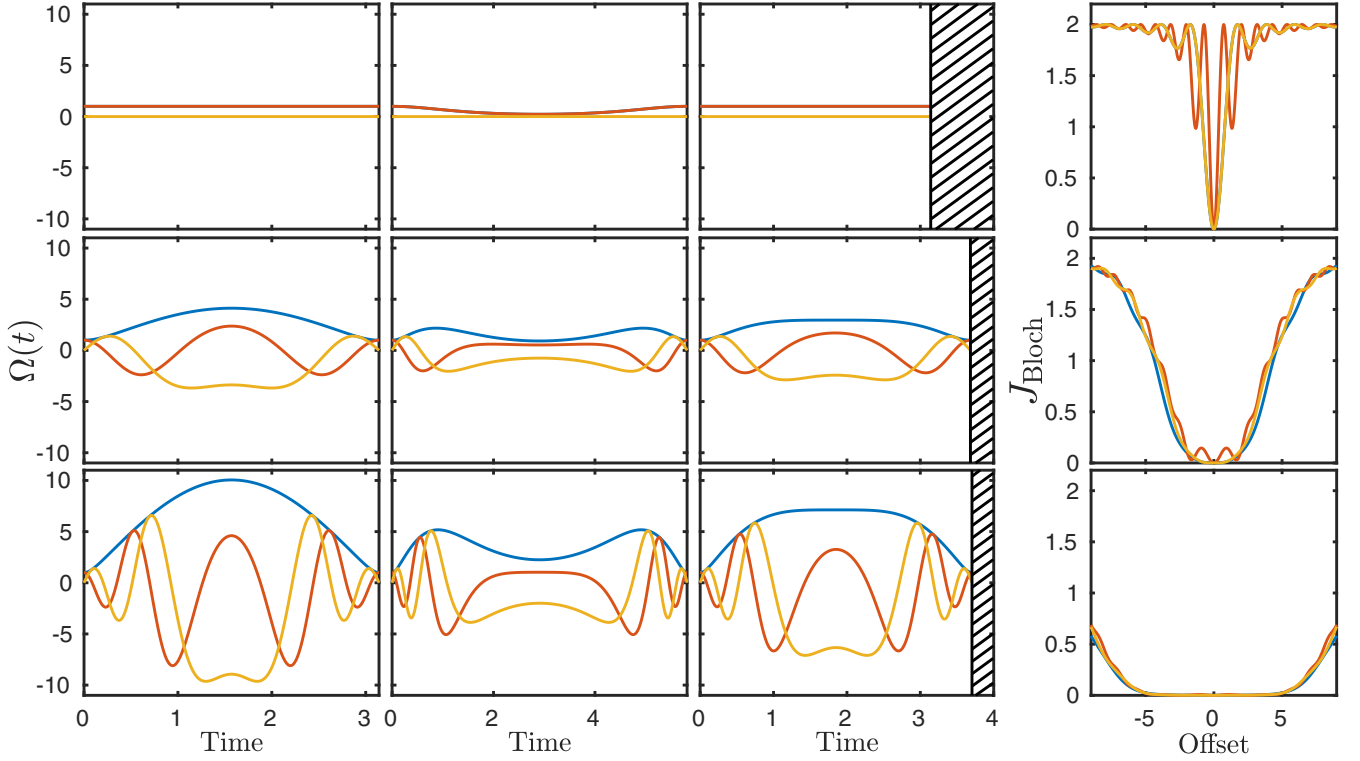


FIG. 2. First column: Anger-Weber (or Jacobi with  $m = 0$ ) pulse amplitude  $\Omega(t)$  (blue or dark-gray line),  $x$  component  $\Omega \cos \phi$  (red or gray line) and  $y$  component  $\Omega \sin \phi$  (yellow or light-gray line) computed with Eq. (28) for various values of  $\nu$ . Second column: Jacobi pulse amplitude [Eq. (30)] and components computed for  $m = 0.95$ . Third column: Jacobi pulse amplitude and components computed for  $m = \nu^2/(2\nu^2 + 1)$ . From top to bottom, the values of  $\nu$  are  $\nu = 0$ ,  $\nu = 4$ , and  $\nu = 10$ , respectively. Last column: associated cost profile computed from Eq. (11) for the Anger-Weber pulse (blue or dark gray), the Jacobi pulse with  $m = 0.95$  (red or gray), and the Jacobi pulse with  $m = \nu^2/(2\nu^2 + 1)$  (yellow or light gray). Quantities plotted are dimensionless.

software XMAXIMA to simplify the latter formula. We obtain

$$\begin{aligned}\Omega(t) &= \sqrt{1 + \nu^2 \sin^2 t}, \\ \phi(t) &= \nu \sin t + \arctan(\nu \sin t).\end{aligned}\quad (28)$$

Note that, in the limit  $\nu = 0$ , the pulse is a simple square  $\pi$  pulse of amplitude 1. When  $\nu$  tends to  $\infty$ , this pulse becomes infinitely robust. The left panels of Fig. 2 display the pulse and its efficiency for different values of  $\nu$ .

The Anger-Weber solution is an example that allows one to fully understand the process, but since it depends only on  $\nu$  one cannot control the shape of the pulse for satisfying given experimental constraints. In the following, we present other solutions giving more flexible pulses. However, the cost profile in STA cannot be explicitated in terms of simple functions. We assume that the parameter  $\nu$  has the same effect of improving the robustness without giving rigorous proof. Cost profiles are shown to confirm this assumption.

*Jacobi pulse.* Let us choose the functions  $k_x$ ,  $k_y$ , and  $k_z$  such that

$$\begin{aligned}\frac{dk_x}{ds} &= \frac{\sin s \cos(\nu s)}{\sqrt{1 - m \sin^2 s}}, & \frac{dk_y}{ds} &= \frac{\sin s \sin(\nu s)}{\sqrt{1 - m \sin^2 s}}, \\ \frac{dk_z}{ds} &= \frac{\cos s}{\sqrt{1 - m \sin^2 s}}, & k_z(s) &= \frac{\arcsin[\sqrt{m} \sin(s)]}{\sqrt{m}},\end{aligned}\quad (29)$$

where  $m$  is an arbitrary modulus with  $m \in [0, 1]$ . Here, the cost profile cannot be expressed in terms of simple functions. Indeed, the final transverse magnetization is given by the integral

$$\ell(\delta, T) = i\delta \int_0^T \frac{\sin(s) e^{i(\nu s + \frac{\delta}{\sqrt{m}} \arcsin[\sqrt{m} \sin(s)])}}{\sqrt{1 - m \sin^2 s}} ds.$$

We assume that, for a given  $m$ , increasing  $\nu$  reduces  $|\ell(\delta, T)|$  as for the Anger-Weber solution, resulting in an improvement of the cost profile. To show this feature, the pulse is explicitly derived using Eq. (23) and its performances are computed numerically by integrating the original Bloch equations (1). One can show that the function  $s(t)$  and the pulse are given by

$$\begin{aligned}s(t) &= \text{am}(t, m), \\ \frac{ds}{dt} &= \sqrt{1 - m \sin^2[s(t)]}, \\ \Omega(t) &= \sqrt{1 - m \sin^2[s(t)]} \sqrt{1 + \nu^2 \sin^2[s(t)]}, \\ \phi(t) &= \nu \sin[s(t)] + \arctan\{\nu \sin[s(t)]\}, \\ T &= 2K(m),\end{aligned}\quad (30)$$

where  $K(m)$  is a complete elliptic integral of the first kind and  $\text{am}(t, m)$  is the Jacobi amplitude [66]. In this solution,  $\nu$  improves the robustness profile while the modulus  $m$  can be used to shape the pulse amplitude. Note that the case  $m = 0$  leads to the Anger-Weber solution computed in the previous paragraph. Figure 2 displays some of these pulses together

with their performances. As can be seen, the parameter  $m$  allows one to reduce the maximum amplitude while increasing the time. The particular choice  $m = v^2/(2v^2 + 1)$  involves that  $\Omega(t)$  is very flat about  $t = T/2$ . The reason is that it cancels the second derivative of  $\Omega(t)$  at  $t = T/2$ . The shape of the cost profile is also affected by  $m$ . A deeper study would be necessary to choose a suitable  $m$  for a given offset range and specific experimental constraints.

*Generalized Jacobi pulse.* Many more parameters can be used to shape the pulse. We consider the functions  $k_x$ ,  $k_y$ , and  $k_z$  defined as

$$\begin{aligned} \frac{dk_x}{ds} &= \frac{\sin s \cos(\nu s)}{P_N(s)}, & \frac{dk_y}{ds} &= \frac{\sin s \sin(\nu s)}{P_N(s)}, \\ \frac{dk_z}{ds} &= \frac{\cos s}{P_N(s)}, \end{aligned} \tag{31}$$

where the function  $P_N$  is given by

$$P_N(s) = \sqrt{1 - m_1 \sin^2 s} \sqrt{1 - m_2 \sin^2 s} \cdots \sqrt{1 - m_N \sin^2 s}, \tag{32}$$

and  $m_1, \dots, m_N$  are arbitrary moduli belonging to  $[0,1]$ . The pulse can be expressed as

$$\begin{aligned} s(t) &= \text{am}_N(t, m_1, \dots, m_N), \\ \frac{ds}{dt} &= P_N[s(t)], \\ \Omega(t) &= P_N[s(t)] \sqrt{1 + v^2 \sin^2[s(t)]}, \\ \phi(t) &= \nu \sin[s(t)] + \arctan\{\nu \sin[s(t)]\}, \\ T &= 2K_N(m), \end{aligned} \tag{33}$$

where  $\text{am}_N(t, m_1, \dots, m_N)$  is the generalized Jacobi amplitude and  $K_N$  the generalized elliptic integral of the first kind (see Ref. [68] for a complete description of these functions in the case  $N = 2$  and Appendix B for the necessary properties). Again, increasing  $\nu$  improves the robustness, while the extra parameters  $m_i$  can be used to shape the pulse.

*Amplitude-fixed pulse.* From a practical point of view, it is often necessary to have a pulse with a constant amplitude set by the experimental setup. This constraint can be satisfied by choosing the following parametrization of the functions  $k_i$ :

$$\begin{aligned} \frac{dk_x}{ds} &= \sqrt{1 + v^2} \sin s \cos \left\{ \nu \ln \left[ \tan \left( \frac{s}{2} \right) \right] \right\}, \\ \frac{dk_y}{ds} &= \sqrt{1 + v^2} \sin s \sin \left\{ \nu \ln \left[ \tan \left( \frac{s}{2} \right) \right] \right\}, \\ \frac{dk_z}{ds} &= \sqrt{1 + v^2} \cos s. \end{aligned} \tag{34}$$

Indeed, applying Eqs. (23) leads to a pulse of the form

$$\begin{aligned} s(t) &= t/\sqrt{1 + v^2}, \\ \Omega(t) &= 1, \\ \phi(t) &= \nu \ln\{\sin[s(t)]\}, \\ T &= \pi\sqrt{1 + v^2}. \end{aligned} \tag{35}$$

The parameter  $\nu$  improves the robustness by changing only the duration and the phase of the pulse, while keeping the amplitude equal to 1. Figure 3 depicts some pulses and their performance. The case  $\nu = 0$  is a standard square  $\pi$  pulse, which can be used as a reference for comparing the efficiency of the different pulses. Note that the phase is a fast oscillating function at the beginning and the end of the pulse. If

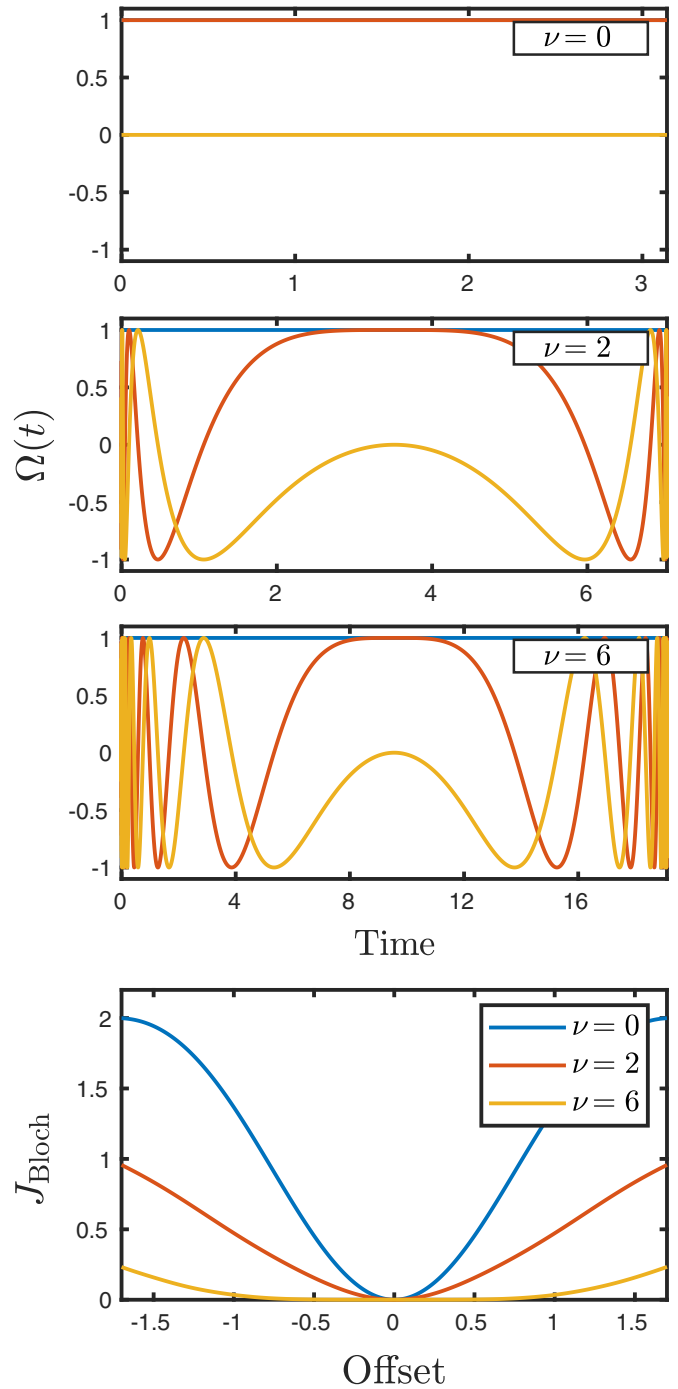


FIG. 3. Three upper panels: amplitude-fixed pulse given by Eq. (35) for various values of  $\nu$ . The blue (dark gray) line represents the amplitude  $\Omega(t) = 1$ , the red (gray) line  $\Omega \cos \phi$ , and the yellow (light-gray) line  $\Omega \sin \phi$ . Lower panel: cost profile associated to each pulse. Quantities plotted are dimensionless.

necessary, these parts can be truncated while keeping a good robustness.

Many more solutions, maybe simpler or more efficient, could be derived easily using this method. As long as the functions  $k_x$ ,  $k_y$ , and  $k_z$  satisfy the boundary constraints, the inversion is realized at the resonance, i.e., for  $\delta = 0$ . Since

many functions satisfy the boundary constraints, we can construct an infinity of pulses with robust properties.

### B. Local robustness and orthogonal polynomial solutions

The pulses presented in the previous section have been derived by guessing that, if  $dk_x/ds$  and  $dk_y/ds$  oscillate with a high frequency, the integral (19) is small over a large range of offset, leading to a good robustness profile. Let us now consider the problem of local robustness that has been introduced in Sec. II D. We show that this problem can be solved by using *orthogonal polynomials* in the interval  $[-1, 1]$ , which have the following property:

$$\int_{-1}^1 v(x)p_n(x)p_m(x)dx = 0 \quad \text{if } n \neq m, \quad (36)$$

where  $v(x)$  is called the weight function and  $p_n$  is a polynomial of degree  $n$ . While many families of orthogonal polynomials could be used, we prefer to focus on one solution based on Chebyshev polynomials of the first and second kinds. The function  $s$  fulfills

$$s_0 = -1 \rightarrow s_T = 1, \quad (37)$$

and we consider functions  $k_x$ ,  $k_y$ , and  $k_z$  that satisfy

$$\begin{aligned} \frac{dk_x}{ds} &= (1-s^2)\sqrt{1-s^2}U_{2n}(s), & \frac{dk_y}{ds} &= (1-s^2)T_{2n+1}(s), \\ \frac{dk_z}{ds} &= -2s, & k_z(s) &= 1-s^2, \end{aligned} \quad (38)$$

where  $T_n$  and  $U_n$  are Chebyshev polynomials of the first and second kinds, respectively [66]. Note that the boundary constraints (22) are satisfied for an inversion process. The transverse term given by Eq. (19) becomes

$$\begin{aligned} \ell(\delta, T) &= i\delta \int_{-1}^1 (1-s^2)(\sqrt{1-s^2}U_{2n}(s) + iT_{2n+1}(s)) \\ &\quad \times e^{i\delta(1-s^2)} ds. \end{aligned} \quad (39)$$

Considering  $\delta$  as a small perturbation, the exponential function can be truncated up to an arbitrary order  $N$ . We obtain

$$\begin{aligned} \ell^{(N)}(\delta, T) &= \sum_{k=1}^N \frac{(i\delta)^k}{(k-1)!} \int_{-1}^1 (\sqrt{1-s^2}U_{2n}(s) + iT_{2n+1}(s)) \\ &\quad \times (1-s^2)^k ds. \end{aligned} \quad (40)$$

The problem is then to cancel  $N$  integrals that are given by

$$C_k = \int_{-1}^1 (\sqrt{1-s^2}U_{2n}(s) + iT_{2n+1}(s))(1-s^2)^k ds, \quad (41)$$

for  $k = \{1, \dots, N\}$ . Note that each term  $(1-s^2)^k$  is a symmetric function on  $[-1, 1]$ . Moreover, the polynomial  $T_{2n+1}(s)$  is antisymmetric, which involves that the imaginary part of  $C_k$  cancels for all  $k$ . Since  $(1-s^2)^k$  is a polynomial of order  $2k$  and  $U_{2k}$  is also a polynomial of order  $2k$ , each term  $(1-s^2)^k$  can be expressed as a linear combination of  $\{U_{2k}, U_{2k-1}, \dots, U_0\}$ . In other words, each integral (41) can

be written as

$$C_k = \sum_{\ell=1}^{2k} a_\ell \int_{-1}^1 \sqrt{1-s^2}U_{2n}(s)U_\ell(s)ds, \quad (42)$$

for  $k = \{1, \dots, N\}$  and where the  $a_\ell$ 's are some coefficients that can be derived using a Chebyshev expansion, which is not necessary here. The weight function of the Chebyshev polynomials  $U_k(s)$  is given by  $\sqrt{1-s^2}$ . Therefore, using the orthogonality property (36) and choosing  $n = N + 1$ , all the terms of the sum cancel for every  $k$ , i.e.,

$$C_k = 0 \quad \forall k \in \{1, \dots, N\}, \quad (43)$$

and the problem is solved.

The final step consists in computing the associated pulse. The details of the computation can be found in Appendix C. We obtain

$$\begin{aligned} s(t) &= \left[ \sqrt{1 + \frac{(4-3t)^2}{4}} - \frac{4-3t}{2} \right]^{\frac{1}{3}} \\ &\quad - \left[ \sqrt{1 + \frac{(4-3t)^2}{4}} + \frac{4-3t}{2} \right]^{\frac{1}{3}}, \\ \Omega(t) &= \frac{\sqrt{4 + (2n+1)^2[1-s^2(t)]}}{[1+s^2(t)]^2}, \\ \phi(t) &= \sqrt{2}(2n+1)\operatorname{arctanh}\left(\sqrt{\frac{1-s^2(t)}{2}}\right) \\ &\quad + \arctan\left(\frac{(2n+1)\sqrt{1-s^2(t)}}{2}\right), \\ T &= 8/3. \end{aligned} \quad (44)$$

Choosing  $n = 2$  for this pulse cancels the first order perturbation term, i.e., the integral  $C_1$ . For  $n = 3$ , the integrals  $C_1$  and  $C_2$  are nullified, while, in the case  $n = 4$ ,  $C_1$ ,  $C_2$ , and  $C_3$  are zero, and so on. Generally, choosing  $n = N + 1$  cancels the integrals  $C_1$  to  $C_N$ . The robustness is then locally improved up to an arbitrary order. Figure 4 shows the pulse for different values of  $n$  and the associated cost computed by propagating numerically the original Bloch equation (1). A linear and a logarithmic scale is used for the cost profile to emphasize the very high precision of the transfer close to  $\delta = 0$ .

### C. Arbitrary flip angle excitation pulses

In this section, we generalize the method of local robustness to any flip angle excitation transfer. As explained in Sec. II, the transfer is fixed by the final constraint  $\vec{v}(T)$ . For a target flip angle  $\theta_T$ , the constraint is  $\vec{v}(T) = (\sin[\theta_T], 0, \cos[\theta_T])^\top$ . With the change of variable  $t \rightarrow s(t)$ , the constraints (22) become

$$\begin{aligned} \frac{dk_x}{ds} &= 0, & \frac{dk_y}{ds} &= 0, & \frac{dk_z}{ds} &> 0 \quad \text{at } s = s_0, \\ \frac{dk_x}{ds} &= A \sin \theta_T, & \frac{dk_y}{ds} &= 0, & \frac{dk_z}{ds} &= A \cos \theta_T \quad \text{at } s = s_T, \end{aligned} \quad (45)$$

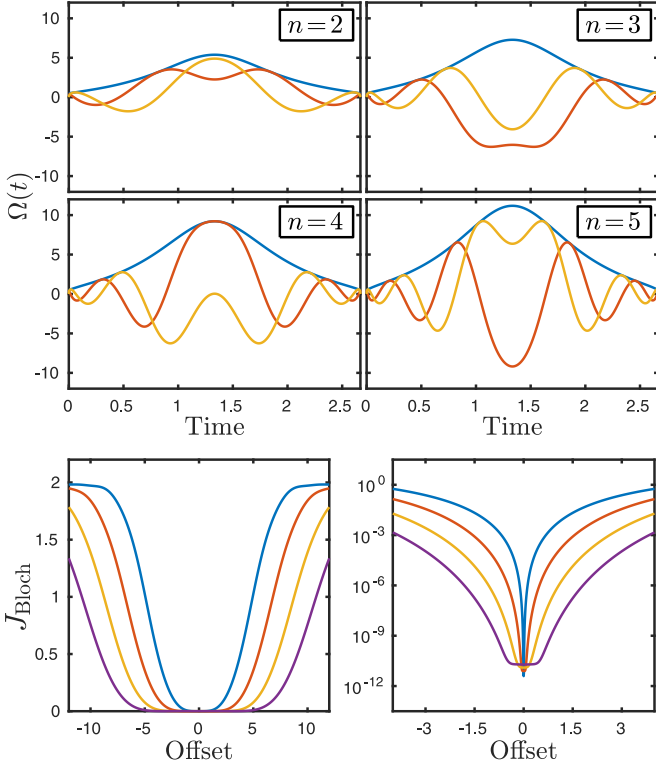


FIG. 4. Upper panels: pulse amplitude  $\Omega(t)$  (blue or dark-gray line),  $x$  component  $\Omega \cos \phi$  (red or gray line), and  $y$  component  $\Omega \sin \phi$  (yellow or light-gray line) computed with Eq. (44) for  $n = 2, 3, 4$ , and  $5$ . Lower panels: cost computed with Eq. (11) associated to  $n = 2$  (blue or dark gray),  $n = 3$  (red or gray),  $n = 4$  (yellow or light gray), and  $n = 5$  (purple or black). The right panel represents the profile in a logarithmic scale. Quantities plotted are dimensionless.

where  $A$  is an arbitrary multiplicative constant coming from the fact that  $\|d\vec{k}/ds\|$  does not need to be equal to 1, unlike  $\|\vec{v}\|$ . We define the bounds of the function  $s$  as

$$s_0 = -1 \rightarrow s_T = 1.$$

For the inversion process, the pulse symmetry allows us to derive analytically the pulse. For other state to state transfers, this trick cannot be used and both  $dk_x/ds$  and  $dk_y/ds$  have to be chosen such that each integral (18) cancels due to the orthogonal properties of the polynomials (in Sec. III B,  $dk_y/ds$  is antisymmetric which ensures that the imaginary part of the integrals cancels). Additional difficulties then appear in computing the pulse, as shown below.

Let us choose the functions  $k_x$ ,  $k_y$ , and  $k_z$ , such that

$$\begin{aligned} \frac{dk_x}{ds} &= \frac{(1+s)\sin\theta_T}{2} [P_n^{(0,1)}(s) + P_{n+1}^{(0,1)}(s)], \\ \frac{dk_y}{ds} &= \frac{(1+s)(n+1)}{2} [P_n^{(0,1)}(s) - P_{n+1}^{(0,1)}(s)], \\ \frac{dk_z}{ds} &= 2 \left[ \cos^2\left(\frac{\theta_T}{2}\right) - s \sin^2\left(\frac{\theta_T}{2}\right) \right], \\ k_z(s) &= (1+s)^2 \cos^2\left(\frac{\theta_T}{2}\right) + 1 - s^2, \end{aligned} \quad (46)$$

where  $P_n^{(a,b)}$  is a Jacobi polynomial [66]. The weight function of this polynomial being  $(1-s)^a(1+s)^b$ , we can show that an  $N$ th order robust control can be found by choosing

$$n = 2N - 1. \quad (47)$$

The function  $s(t)$  cannot be explicitly found in this case because it is given by the inverse of the following integral:

$$\begin{aligned} dt &= \sqrt{\left(\frac{dk_x}{ds}\right)^2 + \left(\frac{dk_y}{ds}\right)^2 + \left(\frac{dk_z}{ds}\right)^2} ds \\ \Rightarrow t(s) &= \int_{-1}^s \sqrt{\left(\frac{dk_x}{ds}\right)^2 + \left(\frac{dk_y}{ds}\right)^2 + \left(\frac{dk_z}{ds}\right)^2} ds \equiv F(s) \\ \Rightarrow s(t) &= F^{-1}(t), \end{aligned} \quad (48)$$

which cannot be computed analytically. However, the computation of  $s(t)$  can be easily done numerically. Indeed,  $t(s)$  is always monotonous since it is the integral of a positive function. Thus its inverse is simply the symmetric of  $F(t)$  with respect to the line of equation  $t = s$ . The second derivative of  $\vec{k}(s)$  is given by

$$\begin{aligned} \frac{d^2k_x}{ds^2} &= \frac{\sin\theta_T}{2} [P_n^{(0,1)}(s) + P_{n+1}^{(0,1)}(s)] \\ &\quad + \frac{(1+s)\sin\theta_T}{4} [(n+2)P_{n-1}^{(1,2)}(s) + (n+3)P_n^{(1,2)}(s)], \\ \frac{d^2k_y}{ds^2} &= \frac{n+1}{2} [P_n^{(0,1)}(s) - P_{n+1}^{(0,1)}(s)] \\ &\quad + \frac{(1+s)(n+1)}{4} [(n+2)P_{n-1}^{(1,2)}(s) - (n+3)P_n^{(1,2)}(s)], \\ \frac{d^2k_z}{ds^2} &= -2 \sin^2\left(\frac{\theta_T}{2}\right), \end{aligned} \quad (49)$$

and the third derivative is

$$\begin{aligned} \frac{d^3k_x}{ds^3} &= \frac{\sin\theta_T}{2} [(n+2)P_{n-1}^{(1,2)}(s) + (n+3)P_n^{(1,2)}(s)] + \frac{(1+s)(n+3)\sin\theta_T}{8} [(n+2)P_{n-2}^{(2,3)}(s) + (n+3)P_{n-1}^{(2,3)}(s)], \\ \frac{d^3k_y}{ds^3} &= \frac{(n+1)}{2} [(n+2)P_{n-1}^{(1,2)}(s) - (n+3)P_n^{(1,2)}(s)] + \frac{(1+s)(n+3)(n+1)}{8} [(n+2)P_{n-2}^{(2,3)}(s) - (n+3)P_{n-1}^{(2,3)}(s)], \\ \frac{d^3k_z}{ds^3} &= 0. \end{aligned} \quad (50)$$

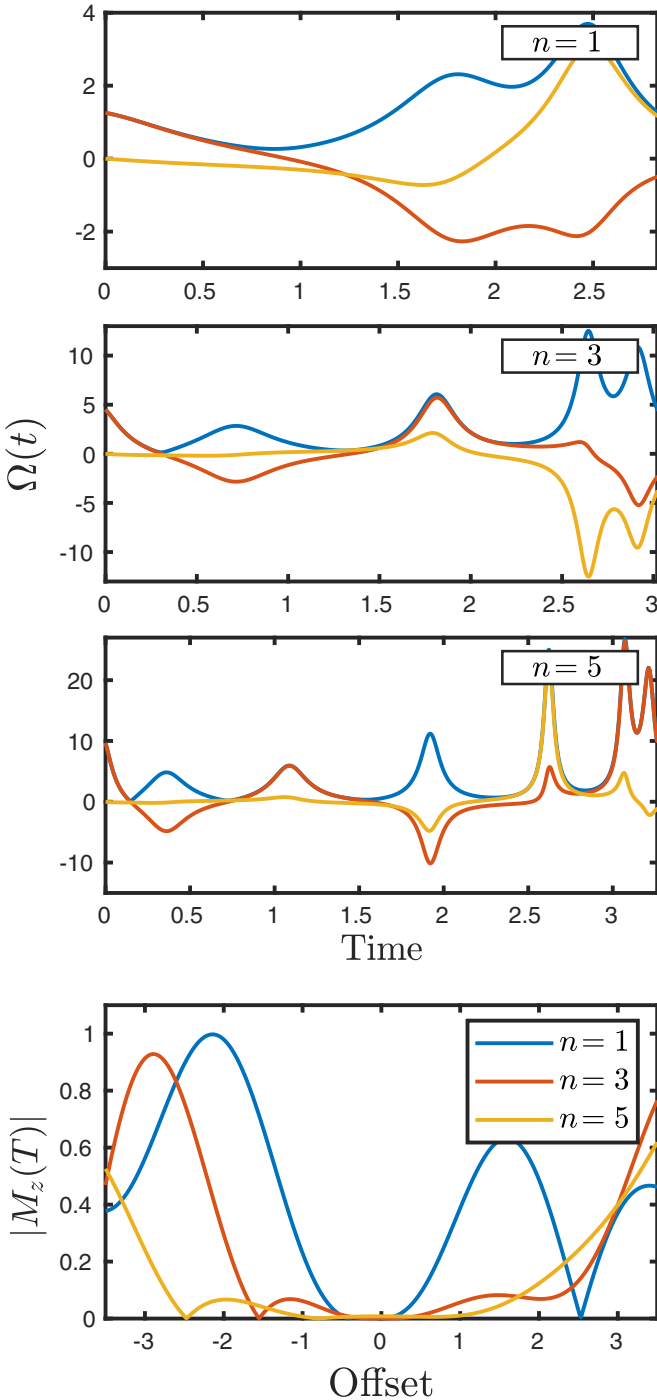


FIG. 5. Excitation pulse ( $\theta_T = 90^\circ$ ) robust up to the first ( $n = 1$ ), second ( $n = 3$ ), and third ( $n = 5$ ) orders and associated excitation cost profile. Quantities plotted are dimensionless.

For  $n = 1$ , the terms  $P_{n-2}^{(2,3)}$  are zero. The pulse is then given by Eq. (23), which cannot be simplified. Unfortunately, we do not find any function  $\vec{k}(s)$  that allows one to derive a simple analytic pulse as for the inversion process. Moreover, finding polynomials that lead to some pulses of low amplitude seems to be difficult in this context. Figure 5 displays the pulses that cancel the offset inhomogeneities up to the third order for a  $\theta_T = 90^\circ$  excitation transfer. As can be seen, the amplitude of the pulse becomes very large when the robustness increases,

as compared to Fig. 4. However, note that these pulses are of finite amplitude, i.e., they are not Dirac functions.

## IV. NUMERICAL ANALYSIS

### A. Comparison with GRAPE

This section compares the preceding results with a robust inversion pulse optimized with the GRAPE algorithm [23]. GRAPE is a gradient-based optimization algorithm which uses piecewise constant pulses. We consider time steps of  $\Delta\tau = 0.5 \mu\text{s}$  and amplitude-constant pulses of amplitude  $v_{\text{max}} = 10 \text{ kHz}$  as in Refs. [37,39] corresponding to

$$\omega_{\text{max}} = 2\pi \times 10^4 \text{ rad/s.}$$

We make a comparison with the amplitude-fixed pulse presented in Sec. III [Eq. (35)], which is properly scaled by applying the formula

$$s(\tau) = \omega_{\text{max}} \tau / \sqrt{1 + v^2}, \quad \Omega_p(\tau) = \omega_{\text{max}},$$

$$\phi(\tau) = v \ln\{\sin[s(\tau)]\}, \quad T_p = \pi \sqrt{1 + v^2} / \omega_{\text{max}}, \quad (51)$$

where  $\tau$  is the time in seconds,  $T_p$  is the pulse duration, and  $\Omega_p$  is the pulse amplitude in rad/s. We consider a pulse of duration  $T_p = 250 \mu\text{s}$  by choosing  $v = 4.8990$ . The numerical pulse is of the same duration and is optimized over an offset range  $\delta \in [-\omega_{\text{max}}, \omega_{\text{max}}]$ . The algorithm is initialized using Eq. (51) and is aimed to minimize the average of the cost function [Eq. (3)] over the aforementioned range of offsets, i.e.,

$$\mathcal{J} = \int_{-\omega_{\text{max}}}^{\omega_{\text{max}}} [1 + M_z(\delta, T)] d\delta.$$

The resulting pulse and the cost profile are shown in Fig. 6. As expected, the numerical pulse is more efficient over the offset optimization range. However, the cost increases faster outside of this box. This feature can be explained by the fact that the amplitude-fixed pulse cannot be optimized over a certain offset range since the only degree of freedom  $v$  is used to set the pulse duration. In contrast, GRAPE uses all the available pulse energy to improve the cost within the optimization range.

### B. Comparison with AHT

A very interesting question would be to know if our method could be used to derive such optimal pulses. If so, one should have to apply the Pontryagin maximum principle [17] within this framework, which involves more complexity. However, this issue can be partially answered by verifying the validity of our approximation for an optimal pulse by inverting the general procedure, i.e., by (i) computing  $\vec{v}(t)$  numerically from the optimal pulse, (ii) computing  $\ell(\delta, T)$  from Eq. (15), (iii) computing the cost profile under STA from Eq. (16), and (iv) comparing it to the cost profile measured in TF (11) determined numerically. The approximation is valid as long as the exact cost profile is well approximated. Figure 7 displays the cost profile of the GRAPE pulse with and without the small-tip-angle approximation. As can be seen in Fig. 6, STA is relevant over a range  $\delta/2\pi \in [-4 \text{ kHz}, 4 \text{ kHz}]$  and becomes completely wrong outside this range. It does not

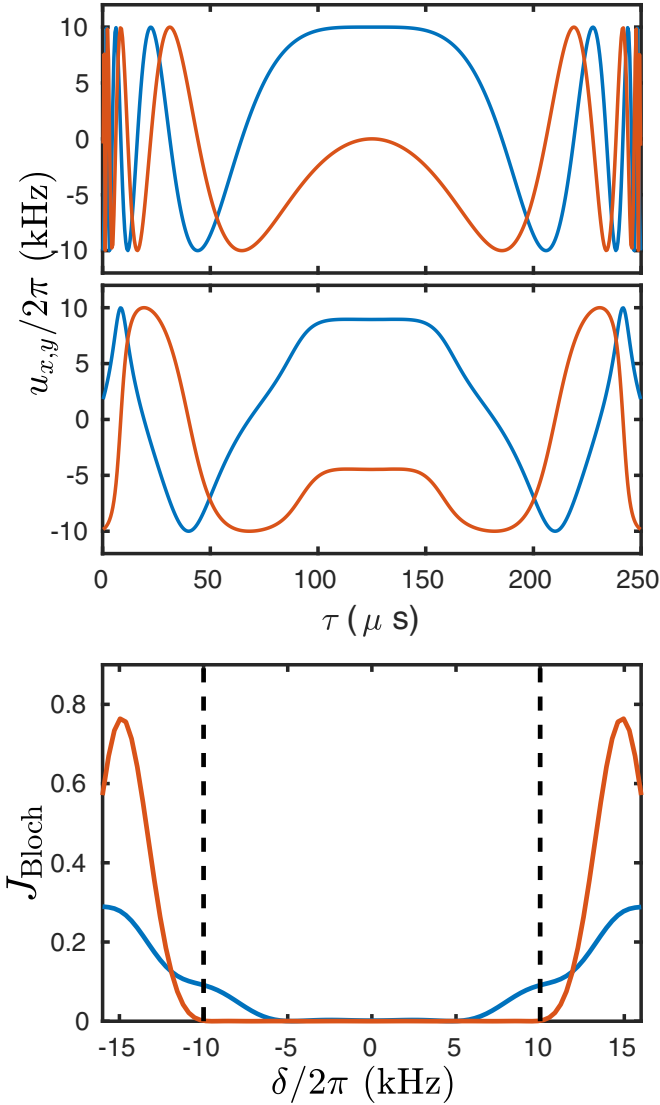


FIG. 6. Upper panel: plot of the  $x$  component (blue or dark-gray line) and of the  $y$  one (red or gray line) of the amplitude fixed pulse given by Eq. (51). Middle panel: plot of the  $x$  and  $y$  components of the GRAPE pulse. Lower panel: cost profile associated to the amplitude-fixed pulse (blue or dark-gray line) and to the GRAPE pulse (red or gray line). The dotted black lines represent the limits of the GRAPE optimization range ( $\pm\omega_{\max}/2\pi$ ).

cover the whole optimization offset range in this case. This feature, however, depends on the dynamics and on the pulse. A complete study would be necessary to figure out in which conditions our approximation holds. A possible approach could be to use the method of Ref. [48] in TF.

As a comparison, we compute the cost profile by using AHT in TF up to the first order of the Magnus expansion. The second order would have to be compared to a second-order STA, which would involve much more complexity. The cost profile obtained with AHT can be done by computing  $\tilde{L}(\delta, T)$  from  $\tilde{v}(t)$  through the formula

$$\tilde{L}(\delta, T) = U(\delta, T)\tilde{L}(\delta, 0), \quad (52)$$

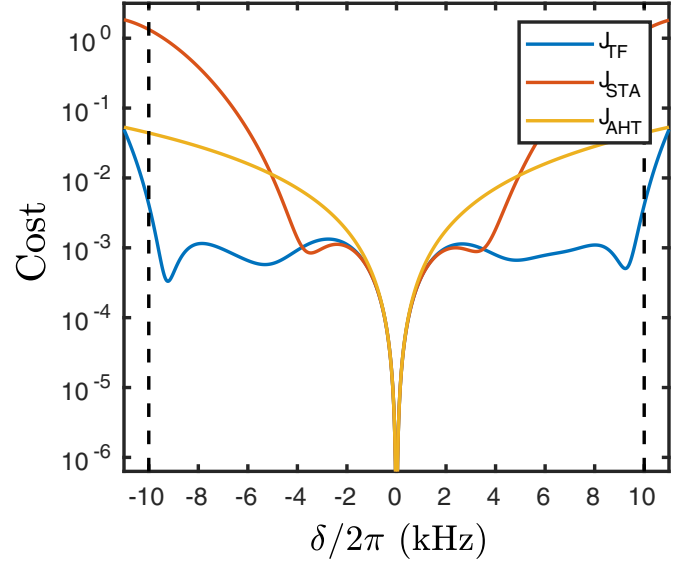


FIG. 7. Logarithmic view of the cost profile resulting from the GRAPE pulse, obtained using a numerical propagation and Eq. (11) (blue or dark gray), using the STA approximation and Eq. (16) (red or gray), and using the AHT theory (yellow or light gray). The dotted black lines represent the limits of the optimization range of the GRAPE pulse.

with  $\tilde{L}(\delta, 0) = (0, 0, 1)^\top$  and

$$U(\delta, T) = \exp \left[ \delta \int_0^T \tilde{H}_1(t) dt \right], \quad (53)$$

where  $\tilde{H}_1(t)$  is the  $3 \times 3$  matrix given by Eq. (6). The cost profile is then given by  $J_{\text{AHT}}(\delta) = 1 - L_z(\delta, T)$ . We can see on Fig. 7 that STA is valid over a larger range of offset than AHT, the latter being relevant for  $\delta/2\pi \in [-2 \text{ kHz}, 2 \text{ kHz}]$ . STA is thus a better tool here, but is still not enough to study the properties of the pulse over the whole optimization range. In fact, our results suggest that STA is more relevant for long duration robust pulses, while AHT theory is a better approximation for short pulses.

## V. CONCLUSION

We apply in this study the small-tip-angle approximation in the toggling frame for the design of robust state to state transfers against offset inhomogeneities. Despite the apparent complexity of the method, a series of analytic and experimentally relevant pulses have been derived. Even if the final state of each system cannot be generally found analytically due to the complexity of the dynamics, the application of STA allows us to express the cost profile through a simple integral that can be computed explicitly in some cases. This approximation is particularly relevant for local robustness (small offset range) and for long duration pulses with a good performance over a large offset range. Although only a few pulses are explicated in this paper, the method can be used to derive an infinite number of analytic pulses with different properties that could be adapted to specific experimental constraints. Other state to state transfers than the inversion process bring up additional

difficulties for calculating analytic pulses with a reasonable amplitude.

While STA is well known for state to state transfer in quantum control and in NMR, it could also be used here for unitary transformations. Indeed, it allows one to derive the flip angle and the azimuthal angle as a function of time, that is two of the three required angles for deriving the propagator of the transformation. The third angle can be expressed as a function of the two other angles at least implicitly through an integral. Thus the application to unitary transformation would involve more complexity, but could also be a better approximation than AHT theory. Another extension of this approach is to consider  $B_1$ -field inhomogeneities. In this case, the function  $\bar{v}(t)$  is replaced by other functions with different properties, which stems from the fact that the interaction Hamiltonian changes. A more complex study would be to apply this method to a coupled spins system, similar to Ref. [69] for state to state control problems.

### ACKNOWLEDGMENTS

This research project has received funding from the European Union's Horizon 2020 research and innovation programme under the Marie-Sklodowska-Curie Grant Agreement No. 765267 (QUSCO). S.J.G. and L.V.D. acknowledge support from the Deutsche Forschungsgemeinschaft (DFG, German Research Foundation) under Germany's Excellence Strategy, Grant No. EXC-2111–390814868.

### APPENDIX A: DERIVATION OF EQS. (23)

These equations are obtained from Eq. (8). Using the fact that  $\bar{v} = \frac{d\bar{k}}{dt} = \frac{d\bar{k}}{ds} \frac{ds}{dt}$ , we have

$$\frac{d\bar{v}}{dt} = \frac{d}{dt} \left( \frac{d\bar{k}}{ds} \frac{ds}{dt} \right) = \frac{d}{ds} \left( \frac{d\bar{k}}{ds} \frac{ds}{dt} \right) \frac{ds}{dt}. \quad (\text{A1})$$

Since  $\frac{ds}{dt} = \left\| \frac{d\bar{k}}{ds} \right\|^{-1}$  [Eq. (20)], we arrive at

$$\begin{aligned} \frac{d\bar{v}}{dt} &= \frac{d}{ds} \left( \frac{d\bar{k}}{ds} \left\| \frac{d\bar{k}}{ds} \right\|^{-1} \right) \left\| \frac{d\bar{k}}{ds} \right\|^{-1} \\ &= \left[ \left\| \frac{d\bar{k}}{ds} \right\|^{-1} \frac{d^2\bar{k}}{ds^2} - \left( \frac{d}{ds} \left\| \frac{d\bar{k}}{ds} \right\| \right) \left\| \frac{d\bar{k}}{ds} \right\|^{-2} \frac{d\bar{k}}{ds} \right] \left\| \frac{d\bar{k}}{ds} \right\|^{-1}. \end{aligned} \quad (\text{A2})$$

Using  $\frac{d}{ds} \left\| \frac{d\bar{k}}{ds} \right\| = \left( \frac{d\bar{k}}{ds} \cdot \frac{d^2\bar{k}}{ds^2} \right) \left\| \frac{d\bar{k}}{ds} \right\|^{-1}$ , we get

$$\begin{aligned} \frac{d\bar{v}}{dt} &= \left[ \left\| \frac{d\bar{k}}{ds} \right\|^{-1} \frac{d^2\bar{k}}{ds^2} - \left( \frac{d\bar{k}}{ds} \cdot \frac{d^2\bar{k}}{ds^2} \right) \left\| \frac{d\bar{k}}{ds} \right\|^{-3} \frac{d\bar{k}}{ds} \right] \left\| \frac{d\bar{k}}{ds} \right\|^{-1} \\ &= \left[ \left\| \frac{d\bar{k}}{ds} \right\|^2 \frac{d^2\bar{k}}{ds^2} - \left( \frac{d\bar{k}}{ds} \cdot \frac{d^2\bar{k}}{ds^2} \right) \frac{d\bar{k}}{ds} \right] \left\| \frac{d\bar{k}}{ds} \right\|^{-4} \\ &= \left[ \left( \frac{d\bar{k}}{ds} \cdot \frac{d\bar{k}}{ds} \right) \frac{d^2\bar{k}}{ds^2} - \left( \frac{d\bar{k}}{ds} \cdot \frac{d^2\bar{k}}{ds^2} \right) \frac{d\bar{k}}{ds} \right] \left\| \frac{d\bar{k}}{ds} \right\|^{-4}. \end{aligned} \quad (\text{A3})$$

From the vector triple product, the solution becomes

$$\frac{d\bar{v}}{dt} = \left[ \frac{d\bar{k}}{ds} \times \left( \frac{d^2\bar{k}}{ds^2} \times \frac{d\bar{k}}{ds} \right) \right] \left\| \frac{d\bar{k}}{ds} \right\|^{-4}. \quad (\text{A4})$$

Since  $\frac{d\bar{k}}{ds}$  is orthogonal to  $\left( \frac{d^2\bar{k}}{ds^2} \times \frac{d\bar{k}}{ds} \right)$ , we have  $\left\| \frac{d\bar{k}}{ds} \times \left( \frac{d^2\bar{k}}{ds^2} \times \frac{d\bar{k}}{ds} \right) \right\| = \left\| \frac{d\bar{k}}{ds} \right\| \left\| \frac{d^2\bar{k}}{ds^2} \times \frac{d\bar{k}}{ds} \right\|$  and we obtain

$$\Omega[s(t)] = \left\| \frac{d\bar{v}}{dt} \right\| = \left\| \frac{d^2\bar{k}}{ds^2} \times \frac{d\bar{k}}{ds} \right\| \left\| \frac{d\bar{k}}{ds} \right\|^{-3}, \quad (\text{A5})$$

according to the first equation of (23).

The derivation of the pulse's phase requires one to compute the second derivative  $\ddot{\bar{v}}$ . We have

$$\frac{d^2\bar{v}}{dt^2} = \frac{d}{ds} \left( \frac{d\bar{v}}{dt} \right) \frac{ds}{dt} \quad (\text{A6})$$

$$= \frac{d}{ds} \left[ \frac{d\bar{k}}{ds} \times \left( \frac{d^2\bar{k}}{ds^2} \times \frac{d\bar{k}}{ds} \right) \right] \left\| \frac{d\bar{k}}{ds} \right\|^{-5} \quad (\text{A7})$$

$$\begin{aligned} &= \left[ \frac{d^2\bar{k}}{ds^2} \times \left( \frac{d^2\bar{k}}{ds^2} \times \frac{d\bar{k}}{ds} \right) + \frac{d\bar{k}}{ds} \right. \\ &\quad \left. \times \left( \frac{d^3\bar{k}}{ds^3} \times \frac{d\bar{k}}{ds} \right) \right] \left\| \frac{d\bar{k}}{ds} \right\|^{-5}. \end{aligned} \quad (\text{A8})$$

On the other hand, we have

$$\begin{aligned} \bar{v} \times \dot{\bar{v}} &= \frac{d\bar{k}}{ds} \times \left[ \frac{d\bar{k}}{ds} \times \left( \frac{d^2\bar{k}}{ds^2} \times \frac{d\bar{k}}{ds} \right) \right] \left\| \frac{d\bar{k}}{ds} \right\|^{-5} \\ &= \left[ \underbrace{\left[ \frac{d\bar{k}}{ds} \cdot \left( \frac{d^2\bar{k}}{ds^2} \times \frac{d\bar{k}}{ds} \right) \right]}_{=0} \frac{d\bar{k}}{ds} \right. \\ &\quad \left. - \left\| \frac{d\bar{k}}{ds} \right\|^2 \left( \frac{d^2\bar{k}}{ds^2} \times \frac{d\bar{k}}{ds} \right) \right] \left\| \frac{d\bar{k}}{ds} \right\|^{-5} \\ &= \left( \frac{d\bar{k}}{ds} \times \frac{d^2\bar{k}}{ds^2} \right) \left\| \frac{d\bar{k}}{ds} \right\|^{-3}. \end{aligned} \quad (\text{A9})$$

Thus

$$(\bar{v} \times \dot{\bar{v}}) \cdot \ddot{\bar{v}} = \left( \frac{d\bar{k}}{ds} \times \frac{d^2\bar{k}}{ds^2} \right) \cdot \left[ \frac{d\bar{k}}{ds} \times \left( \frac{d^3\bar{k}}{ds^3} \times \frac{d\bar{k}}{ds} \right) \right] \left\| \frac{d\bar{k}}{ds} \right\|^{-8}. \quad (\text{A10})$$

From the vector triple product, we get

$$\begin{aligned} (\bar{v} \times \dot{\bar{v}}) \cdot \ddot{\bar{v}} &= \frac{d\bar{k}}{ds} \cdot \left[ \left( \frac{d^3\bar{k}}{ds^3} \times \frac{d\bar{k}}{ds} \right) \times \left( \frac{d^2\bar{k}}{ds^2} \times \frac{d\bar{k}}{ds} \right) \right] \left\| \frac{d\bar{k}}{ds} \right\|^{-8} \\ &= \left[ \left( \frac{d\bar{k}}{ds} \times \frac{d^2\bar{k}}{ds^2} \right) \cdot \frac{d^3\bar{k}}{ds^3} \right] \left( \frac{d\bar{k}}{ds} \cdot \frac{d\bar{k}}{ds} \right) \left\| \frac{d\bar{k}}{ds} \right\|^{-8} \\ &= \left[ \left( \frac{d\bar{k}}{ds} \times \frac{d^2\bar{k}}{ds^2} \right) \cdot \frac{d^3\bar{k}}{ds^3} \right] \left\| \frac{d\bar{k}}{ds} \right\|^{-6}. \end{aligned} \quad (\text{A11})$$

Thus

$$\frac{(\vec{v} \times \dot{\vec{v}}) \cdot \ddot{\vec{v}}}{\Omega^2} = \frac{\left(\frac{d\vec{k}}{ds} \times \frac{d^2\vec{k}}{ds^2}\right) \cdot \frac{d^3\vec{k}}{ds^3}}{\left\|\frac{d^2\vec{k}}{ds^2} \times \frac{d\vec{k}}{ds}\right\|^2}. \quad (\text{A12})$$

Finally, we obtain

$$\phi[s(t)] = \int_0^t \frac{\left(\frac{d\vec{k}}{ds} \times \frac{d^2\vec{k}}{ds^2}\right) \cdot \frac{d^3\vec{k}}{ds^3}}{\left\|\frac{d^2\vec{k}}{ds^2} \times \frac{d\vec{k}}{ds}\right\|^2} dt' \quad (\text{A13})$$

$$= \int_{s_0}^s \frac{\left(\frac{d\vec{k}}{ds'} \times \frac{d^2\vec{k}}{ds'^2}\right) \cdot \frac{d^3\vec{k}}{ds'^3}}{\left\|\frac{d^2\vec{k}}{ds'^2} \times \frac{d\vec{k}}{ds'}\right\|^2} ds' \quad (\text{A14})$$

$$= \int_{s_0}^s \frac{\left(\frac{d\vec{k}}{ds'} \times \frac{d^2\vec{k}}{ds'^2}\right) \cdot \frac{d^3\vec{k}}{ds'^3}}{\left\|\frac{d^2\vec{k}}{ds'^2} \times \frac{d\vec{k}}{ds'}\right\|^2} \left\|\frac{d\vec{k}}{ds'}\right\| ds', \quad (\text{A15})$$

according to the second equation of (23).

## APPENDIX B: GENERALIZED ELLIPTIC FUNCTIONS

We recall in this paragraph standard results about elliptic functions.

*Jacobi elliptic functions.* The standard elliptic functions can be defined through the Jacobi amplitude  $\text{am}(u|m)$ , where  $u$  is the argument and  $m$  the modulus such that  $m \in [0, 1]$  [66]. This function is defined as the inverse of an incomplete elliptic integral of the first kind given by

$$F(u|m) = \int_0^u \frac{d\phi}{\sqrt{1-m\sin^2\phi}}. \quad (\text{B1})$$

The Jacobi amplitude  $\text{am}$  is thus related to  $F$  and  $u$  via  $F[\text{am}(u|m)|m] = u$ . The complete elliptic integral  $K(m)$  can then be expressed as  $K(m) = F(\pi/2|m)$ .

*Generalized Jacobi elliptic functions.* A possible generalization of these functions can be constructed through the generalized incomplete elliptic integral of the first kind  $F_n(u|m_1, \dots, m_n)$ , where the  $m_i$ 's are such that  $m_i \in [0, 1]$ ,  $\forall i$ . This integral is defined as

$$F_n(u|m_1, \dots, m_n) = \int_0^u \frac{d\phi}{\sqrt{(1-m_1\sin^2\phi)(1-m_2\sin^2\phi)\cdots(1-m_n\sin^2\phi)}}. \quad (\text{B2})$$

The generalized Jacobi amplitude  $\text{am}_n$  is the inverse of this integral, i.e., it is such that  $F_n(\text{am}_n(u|m_1, \dots, m_n)|m_1, \dots, m_n) = u$ . The complete version of the integral is given by  $K_n(m_1, \dots, m_n) = F_n(\pi/2|m_1, \dots, m_n)$ .

## APPENDIX C: DERIVATION OF EQ. (44)

The derivation of  $s(t)$  is made by using  $\frac{ds}{dt} = \left\|\frac{d\vec{k}(s)}{ds}\right\|^{-1}$ . The property of the Chebyshev polynomials  $(1-s^2)U_{2n}^2 + T_{2n+1}^2 = 1$  involves

$$\frac{ds}{dt} = \frac{1}{\sqrt{\left(\frac{dk_x}{ds}\right)^2 + \left(\frac{dk_y}{ds}\right)^2 + \left(\frac{dk_z}{ds}\right)^2}} = \frac{1}{1+s^2}. \quad (\text{C1})$$

Thus we have

$$t(s) = s + \frac{s^3}{3} + 2, \quad (\text{C2})$$

where the term 2 in the right-hand side of the equation ensures that  $t(s_0) = t(-1) = 0$ . Inverting this relation, we get that  $s(t)$  is given by Eq. (44).

For the computation of the pulse, we start from Eq. (38) that we write here for convenience as

$$\begin{aligned} \frac{dk_x}{ds} &= (1-s^2)\sqrt{1-s^2}U_{2n}(s), \\ \frac{dk_y}{ds} &= (1-s^2)T_{2n+1}(s), \quad \frac{dk_z}{ds} = -2s. \end{aligned} \quad (\text{C3})$$

Differentiating these equations with respect to  $s$  leads to

$$\begin{aligned} \frac{d^2k_x}{ds^2} &= -\sqrt{1-s^2}[(2n+1)T_{2n+1}(s) + 2sU_{2n}(s)], \\ \frac{d^2k_y}{ds^2} &= -2sT_{2n+1}(s) + (2n+1)(1-s^2)U_{2n}(s), \\ \frac{d^2k_z}{ds^2} &= -2, \end{aligned} \quad (\text{C4})$$

and differentiating one more time to

$$\begin{aligned} \frac{d^3k_x}{ds^3} &= \frac{3(2n+1)}{\sqrt{1-s^2}}sT_{2n+1}(s) - [(2n+1)^2 + 2]U_{2n}(s), \\ \frac{d^3k_y}{ds^3} &= -[(2n+1)^2 + 2]T_{2n+1}(s) - 3(2n+1)sU_{2n}(s), \\ \frac{d^3k_z}{ds^3} &= 0. \end{aligned} \quad (\text{C5})$$

The pulse is given by Eq. (23). The cross product between the first and second derivatives of  $\vec{k}$  can be expressed as

$$\begin{aligned} \frac{d\vec{k}}{ds} \times \frac{d^2\vec{k}}{ds^2} &= \begin{pmatrix} -2(1+s^2)T_{2n+1}(s) + 2s(2n+1)(1-s^2)U_{2n}(s) \\ \sqrt{1-s^2}[2s(2n+1)T_{2n+1}(s) + 2(1+s^2)U_{2n}(s)] \\ (2n+1)(1-s^2)^{3/2} \end{pmatrix}. \end{aligned} \quad (\text{C6})$$

We can show that

$$\left\|\frac{d\vec{k}}{ds} \times \frac{d^2\vec{k}}{ds^2}\right\| = (1+s^2)\sqrt{4+(2n+1)^2(1-s^2)}. \quad (\text{C7})$$

The control amplitude being  $\Omega(s) = \left\|\frac{d\vec{k}}{ds} \times \frac{d^2\vec{k}}{ds^2}\right\| \left\|\frac{d\vec{k}}{ds}\right\|^{-3}$ , we obtain Eq. (44).

For the phase of the pulse, we have, in a first step

$$\left(\frac{d\vec{k}}{ds} \times \frac{d^2\vec{k}}{ds^2}\right) \cdot \frac{d^3\vec{k}}{ds^3} = -\frac{2ks[(2n+1)^2(1-s^2) + s^2 + 5]}{\sqrt{1-s^2}}. \quad (\text{C8})$$

Since  $d\phi/ds = \frac{(\frac{d\bar{k}}{ds} \times \frac{d^2\bar{k}}{ds^2}, \frac{d^3\bar{k}}{ds^3})}{\|\frac{d\bar{k}}{ds} \times \frac{d^2\bar{k}}{ds^2}\|^2} \|\frac{d\bar{k}}{ds}\|$ , we have

$$\begin{aligned} \frac{d\phi}{ds} &= -\frac{2ks[(2n+1)^2(1-s^2) + s^2 + 5]}{(1+s^2)\sqrt{1-s^2}[(2n+1)^2(1-s^2) + 4]} \\ &= -\frac{2(2n+1)s}{\sqrt{1-s^2}[(2n+1)^2(1-s^2) + 4]} - \frac{2(2n+1)s}{(1+s^2)\sqrt{1-s^2}}. \end{aligned} \quad (\text{C9})$$

Making the change of variable  $x = s\sqrt{\frac{1-s^2}{2}}$ , we obtain

$$d\phi = \frac{\sqrt{2}}{2+x^2} + \frac{\sqrt{2}}{1-\frac{x^2}{(2n+1)^2}} dx. \quad (\text{C10})$$

Integrating this equation and coming back to the variable  $s$ , we arrive at the formula of Eq. (44).

- 
- [1] P. Brumer and M. Shapiro, *Quantum Control of Molecular Processes*, 2nd, revised, and enlarged ed. (Wiley-VCH, Weinheim, 2012).
- [2] C. P. Koch, M. Lemeshko, and D. Sugny, Quantum control of molecular rotation, *Rev. Mod. Phys.* **91**, 035005 (2019).
- [3] C. Brif, R. Chakrabarti, and H. Rabitz, Control of quantum phenomena: past, present and future, *New J. Phys.* **12**, 075008 (2010).
- [4] S. J. Glaser, U. Boscain, T. Calarco, C. P. Koch, W. Kockenberger, R. Kosloff, I. Kuprov, B. Luy, S. Schirmer, T. Schulte-Herbruggen, D. Sugny, and F. Wilhelm, Training Schrödinger's cat: quantum optimal control, *Eur. Phys. J. D* **69**, 279 (2015).
- [5] M. A. Bernstein, K. F. King, and X. J. Zhou, *Handbook of MRI Pulse Sequences* (Elsevier Academic Press, New York, 2004).
- [6] M. A. Bernstein, K. F. King, and X. J. Zhou, in *Optimal Control Methods in NMR Spectroscopy*, edited by R. K. Harris and R. L. Wasylishen (Wiley, Hoboken, NJ, 2004).
- [7] M. Lapert, Y. Zhang, M. Braun, S. J. Glaser, and D. Sugny, Singular Extremals for the Time-Optimal Control of Dissipative Spin  $\frac{1}{2}$  Particles, *Phys. Rev. Lett.* **104**, 083001 (2010).
- [8] E. Assémat, M. Lapert, Y. Zhang, M. Braun, S. J. Glaser, and D. Sugny, Simultaneous time-optimal control of the inversion of two spin- $\frac{1}{2}$  particles, *Phys. Rev. A* **82**, 013415 (2010).
- [9] N. Khaneja, R. Brockett, and S. J. Glaser, Time optimal control in spin systems, *Phys. Rev. A* **63**, 032308 (2001).
- [10] C. Altafini and F. Ticozzi, Modeling and control of quantum systems: An introduction, *IEEE Trans. Automat. Control* **57**, 1898 (2012).
- [11] D. Dong and I. A. Petersen, Quantum control theory and applications: A survey, *IET Control Theory A* **4**, 2651 (2010).
- [12] N. V. Vitanov, A. A. Rangelov, B. W. Shore, and K. Bergmann, Stimulated Raman adiabatic passage in physics, chemistry, and beyond, *Rev. Mod. Phys.* **89**, 015006 (2017).
- [13] D. Guéry-Odelin, A. Ruschhaupt, A. Kiely, E. Torrontegui, S. Martínez-Garaot, and G. J. Muga, Shortcuts to adiabaticity: Concepts, methods, and applications, *Rev. Mod. Phys.* **91**, 045001 (2019).
- [14] S. Deffner, C. Jarzynski, and A. del Campo, Classical and Quantum Shortcuts to Adiabaticity for Scale-Invariant Driving, *Phys. Rev. X* **4**, 021013 (2014).
- [15] E. Torrontegui, S. Ibanez, S. Martinez-Garaot, M. Modugno, A. del Campo, D. Guery-Odelin, A. Ruschhaupt, X. Chen, and J. G. Muga, Shortcuts to adiabaticity, *Adv. At., Mol., Opt. Phys.* **62**, 117 (2013).
- [16] V. Martikyan, D. Guéry-Odelin, and D. Sugny, Comparison between optimal control and shortcut to adiabaticity protocols in a linear control system, *Phys. Rev. A* **101**, 013423 (2020).
- [17] L. S. Pontryagin, V. G. Boltyanskii, R. V. Gamkrelidze, and E. F. Mishchenko, *Mathematical Theory of Optimal Processes* (Interscience Publishers, New York, 1962).
- [18] U. Boscain, M. Sigalotti, and D. Sugny, Introduction to the Pontryagin maximum principle for quantum optimal control, *PRX Quantum* **2**, 030203 (2021).
- [19] B. Bonnard and D. Sugny, *Optimal Control with Applications in Space and Quantum Dynamics*, AIM Series in Applied Mathematics Vol. 5 (American Institute of Mathematical Sciences, Springfield, MO, 2012).
- [20] A. E. Bryson and Y.-C. Ho, *Applied Optimal Control* (Taylor and Francis, New York, 1975).
- [21] D. D'Alessandro, *Introduction to Quantum Control and Dynamics* (Chapman and Hall, London, 2008).
- [22] D. Reich, M. Ndong, and C. P. Koch, Monotonically convergent optimization in quantum control using Krotov's method, *J. Chem. Phys.* **136**, 104103 (2012).
- [23] N. Khaneja, T. Reiss, C. Kehlet, T. Schulte-Herbruggen, and S. J. Glaser, Optimal control of coupled spin dynamics: Design of nmr pulse sequences by gradient ascent algorithms, *J. Magn. Reson.* **172**, 296 (2005).
- [24] A. Garon, S. J. Glaser, and D. Sugny, Time-optimal control of SU(2) quantum operations, *Phys. Rev. A* **88**, 043422 (2013).
- [25] J. S. Li and N. Khaneja, Ensemble control of Bloch equations, *IEEE Trans. Auto. Control* **54**, 528 (2009).
- [26] B. T. Torosov, B. W. Shore, and N. V. Vitanov, Coherent control techniques for two-state quantum systems: A comparative study, *Phys. Rev. A* **103**, 033110 (2021).
- [27] J. S. Li and N. Khaneja, Control of inhomogeneous quantum ensembles, *Phys. Rev. A* **73**, 030302(R) (2006).
- [28] P. Owrutsky and N. Khaneja, Control of inhomogeneous ensembles on the Bloch sphere, *Phys. Rev. A* **86**, 022315 (2012).
- [29] G. T. Genov, D. Schraft, T. Halfmann, and N. V. Vitanov, Correction of Arbitrary Field Errors in Population Inversion of Quantum Systems by Universal Composite Pulses, *Phys. Rev. Lett.* **113**, 043001 (2014).
- [30] G. T. Genov, M. Hain, N. V. Vitanov, and T. Halfmann, Universal composite pulses for efficient population inversion with an arbitrary excitation profile, *Phys. Rev. A* **101**, 013827 (2020).
- [31] J. A. Jones, Designing short robust NOT gates for quantum computation, *Phys. Rev. A* **87**, 052317 (2013).
- [32] A. Ruschhaupt, X. Chen, D. Alonso, and J. G. Muga, Optimally robust shortcuts to population inversion in two-level quantum systems, *New J. Phys.* **14**, 093040 (2012).

- [33] D. Daems, A. Ruschhaupt, D. Sugny, and S. Guérin, Robust Quantum Control by a Single-Shot Shaped Pulse, *Phys. Rev. Lett.* **111**, 050404 (2013).
- [34] L. Van Damme, D. Schraft, G. T. Genov, D. Sugny, T. Halfmann, and S. Guérin, Robust NOT gate by single-shot-shaped pulses: Demonstration of the efficiency of the pulses in rephasing atomic coherences, *Phys. Rev. A* **96**, 022309 (2017).
- [35] G. Turinici, Stochastic learning control of inhomogeneous quantum ensembles, *Phys. Rev. A* **100**, 053403 (2019).
- [36] C. Chen, D. Dong, R. Long, I. R. Petersen, and H. A. Rabitz, Sampling-based learning control of inhomogeneous quantum ensembles, *Phys. Rev. A* **89**, 023402 (2014).
- [37] K. Kobzar, T. E. Skinner, N. Khaneja, S. J. Glaser, and B. Luy, Exploring the limits of broadband excitation and inversion pulses, *J. Magn. Reson.* **170**, 236 (2004).
- [38] K. Kobzar, B. Luy, N. Khaneja, and S. J. Glaser, Pattern pulses: design of arbitrary excitation profiles as a function of pulse amplitude and offset, *J. Magn. Reson.* **173**, 229 (2005).
- [39] K. Kobzar, S. Ehni, T. E. Skinner, S. J. Glaser, and B. Luy, Exploring the limits of broadband  $90^\circ$  and  $180^\circ$  universal rotation pulses, *J. Magn. Reson.* **225**, 142 (2012).
- [40] M. Lapert, G. Ferrini, and D. Sugny, Optimal control of quantum superpositions in a bosonic Josephson junction, *Phys. Rev. A* **85**, 023611 (2012).
- [41] L. Van Damme, Q. Ansel, S. J. Glaser, and D. Sugny, Robust optimal control of two-level quantum systems, *Phys. Rev. A* **95**, 063403 (2017).
- [42] J. Ruths and J. S. Li, A multidimensional pseudospectral method for optimal control of quantum ensembles, *J. Chem. Phys.* **134**, 044128 (2011).
- [43] J. Ruths and J. S. Li, Optimal control of inhomogeneous ensembles, *IEEE Trans. Auto. Control* **57**, 2021 (2012).
- [44] K. Ugurbil, Imaging at ultrahigh magnetic fields: History, challenges, and solutions, *NeuroImage* **168**, 7 (2017).
- [45] U. Haeblerlen, *High Resolution NMR in Solids. Selective Averaging. Advances in Magnetic Resonance, Supplement 1* (Academic Press, New York, 1976).
- [46] A. Brinkmann, Introduction to average Hamiltonian theory. I. Basics, *Con. Magn. Res. Part A* **45A**, e21414 (2016).
- [47] J. Pauly, D. Nishimura, and A. Macovski, A k-space analysis of small-tip-angle excitation, *J. Magn. Reson.* (1969) **81**, 43 (1989).
- [48] J. S. Li, J. Ruths, and S. J. Glaser, Exact broadband excitation of two-level systems by mapping spins to springs, *Nat. Commun.* **8**, 446 (2017).
- [49] J. Zeng, X. H. Deng, A. Russo, and E. Barnes, General solution to inhomogeneous dephasing and smooth pulse dynamical decoupling, *New J. Phys.* **20**, 033011 (2018).
- [50] J. Zeng and E. Barnes, Fastest pulses that implement dynamically corrected single-qubit phase gates, *Phys. Rev. A* **98**, 012301 (2018).
- [51] J. Zeng, C. H. Yang, A. Dzurack, and E. Barnes, Geometric formalism for constructing arbitrary single-qubit dynamically corrected gates, *Phys. Rev. A* **99**, 052321 (2019).
- [52] M. H. Levitt, *Spin Dynamics: Basics of Nuclear Magnetic Resonance* (Wiley, Chichester, UK, 2008).
- [53] C. Cohen-Tannoudji, B. Diu, and F. Lalo, *Quantum Mechanics*, 1st ed. (Wiley, New York, 1977).
- [54] W. A. Grissom, M. M. Khalighi, L. I. Sacolick, B. K. Rutt, and M. W. Vogel, Small-tip-angle spokes pulse design using interleaved greedy and local optimization methods, *Magn. Res. Med.* **68**, 1553 (2012).
- [55] M. A. Cloos, N. Boulant, M. Luong, G. Ferrand, E. Giacomini, D. Le Bihan, and A. Amadon,  $k_T$ -points: Short three-dimensional tailored RF pulses for flip-angle homogenization over an extended volume, *Magn. Res. Med.* **67**, 72 (2011).
- [56] V. Gras, F. Mauconduit, A. Vignaud, D. Le Bihan, A. Amadon, T. Stocker, and N. Boulant, Design of universal parallel-transmit refocusing  $k_T$ -point pulses and application to 3d t2-weighted imaging at 7t, *Magn. Res. Med.* **80**, 53 (2018).
- [57] S. J. Malik, S. Keihaninejad, A. Hammers, and J. V. Hajnal, Tailored excitation in 3d with spiral nonselective (spins) rf pulses, *Magn. Res. Med.* **67**, 1303 (2012).
- [58] S. Saekho, C. Y. Yip, D. C. Noll, F. E. Boada, and V. A. Stenger, Fast-kz three-dimensional tailored radiofrequency pulse for reduced b1 inhomogeneity, *Magn. Res. Med.* **55**, 719 (2006).
- [59] V. Gras, F. Mauconduit, A. Vignaud, C. Le Ster, L. Leroi, A. Amadon, E. Pracht, M. Boland, R. Stirnberg, T. Stocker, B. A. Poser, C. Wiggins, X. Wu, K. Ugurbil, and N. Boulant, Pasteur: Package of anatomical sequences using parallel transmission universal  $k_T$ -point pulses, in ISMRM 27th 579 annual meeting and exhibition, 2019 (unpublished).
- [60] L. Van Damme, F. Mauconduit, T. Chambrion, N. Boulant, and V. Gras, Universal nonselective excitation and refocusing pulses with improved robustness to off-resonance for magnetic resonance imaging at 7 tesla with parallel transmission, *Magn. Res. Med.* **85**, 678 (2021).
- [61] R. Tycko, E. Schneider, and A. Pines, Broadband population inversion in solid state nmr, *J. Chem. Phys.* **81**, 680 (1984).
- [62] H. K. Cummins, G. Llewellyn, and J. A. Jones, Tackling systematic errors in quantum logic gates with composite rotations, *Phys. Rev. A* **67**, 042308 (2003).
- [63] Wolfram Research, Inc, Mathematica, Version 12.3.1, Champaign, IL, 2021.
- [64] Maxima, Maxima, a computer algebra system. version 5.34.1, 2014.
- [65] Maplesoft, a division of Waterloo Maple Inc., Maple.
- [66] M. Abramowitz and I. A. Stegun, *Handbook of Mathematical Functions* (Dover Publications, Mineola, NY, 1974).
- [67] NIST digital library of mathematical functions, <http://dlmf.nist.gov/>, release 1.1.3 of 2021-09-15, edited by F. W. J. Olver, A. B. Olde Daalhuis, D. W. Lozier, B. I. Schneider, R. F. Boisvert, C. W. Clark, B. R. Miller, B. V. Saunders, H. S. Cohl, and M. A. McClain.
- [68] M. Pawellek, On a generalization of Jacobi's elliptic functions and the double sine-Gordon kink chain, *J. Math. Phys.* **52**, 113701 (2011).
- [69] D. Buterakos, S. Das Sarma, and E. Barnes, Geometrical formalism for dynamically corrected gates in multiqubit systems, *PRX Quantum* **2**, 010341 (2021).